TipA, a *Bdellovibrio bacteriovorus* BPI-like double-TULIP is opened by its adapter protein, TipB.

Simon G. Caulton[1*], Ian T. Cadby[2], Gareth W. Hughes[3], Hannah Johnston[1], Timothy J. Knowles[1], Andrew L. Lovering[1]

Author Affiliations

[1]School of Biosciences, University of Birmingham, Birmingham B15 2TT

[2]Bristol Veterinary School, University of Bristol, Langford, Bristol BS40 5DU, UK

[3]Cancer and Genomic Sciences, University of Birmingham, Birmingham B15 2TT

***corresponding author**

Abstract

Bdellovibrio bacteriovorus is a predatory bacterium that invades the periplasm of other Gram-negative bacteria and liberates prey biomolecules for replication. *Bdellovibrio* has a wealth of genes that encode unique proteins to enable this lifestyle. Using a series of x-ray structures, we show that the operonal pairing of *bd2538* and *bd2539,* encode a double TULIP (tubular lipid binding protein) invasion protein A (TipA) and a small beta sandwich (TipB), respectively. TipA has a specialised N-terminal TULIP domain with a beta hairpin and helix that mediate homodimerisation through hairpin interdigitation. This dimerisation creates a large, continuous, enclosed lumen that we demonstrate to contain multiple lipid molecules. In addition, we show that TipB functions as a small adapter protein that binds to TipA using specialised loops that bury into the TipA hydrophobic core. This binding forms a clamp on the edge of the N-terminal beta sheet and induces a large 20 Å conformational change, opening the TULIP fold to create an accessible interior. This study presents the first structural characterisation of lipid binding proteins in *Bdellovibrio*, and the first example of conformational change in TULIPs mediated by an adaptor protein.

30 **Synopsis**

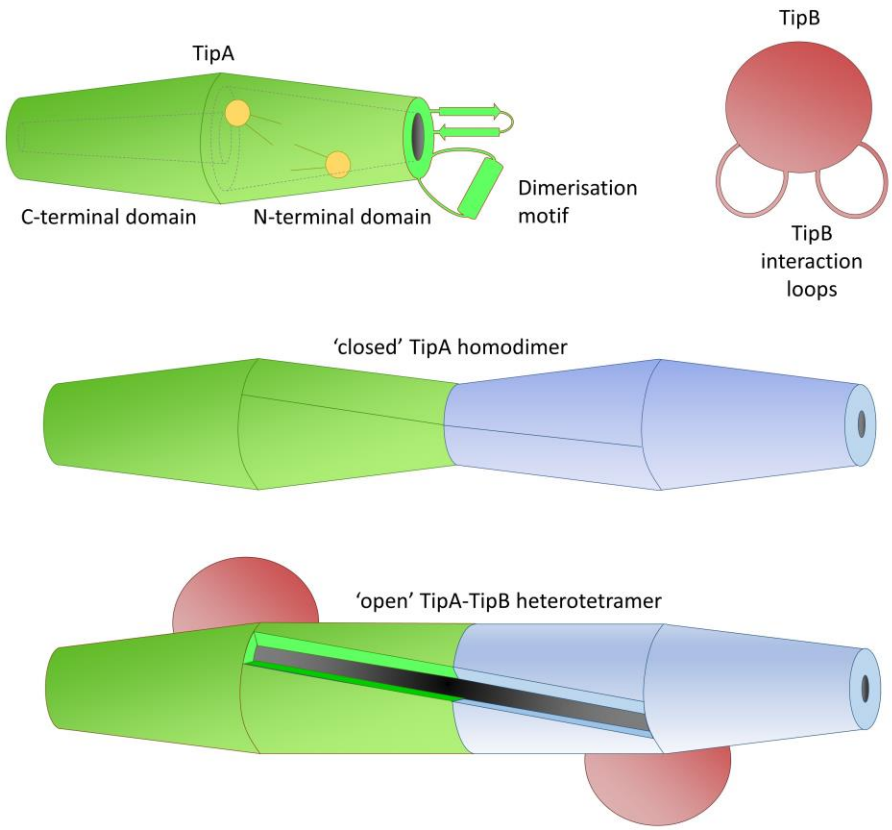

31

32 *Bdellovibrio bacteriovorus* is a predatory bacterium that invades the periplasm of other Gram-
33 negative bacteria in order to consume them from within. To enable this lifestyle, it has an
34 arsenal of predation-associated genes, including the operonal pair *bd2538* and *bd2539*. We use
35 structural and biophysical techniques to characterise two proteins produced by these genes,
36 TipA and TipB.

37

38 • TipA is a double tubular lipid binding protein (TULIP) that forms a homodimer that
39 sequesters lipids in its lumen and binds to lipid bilayers
40 • TipB is a small beta sandwich that interacts with TipA via two specialised loops
41 • Interaction of TipA with TipB opens the TULIP fold of TipA

42

43

44

45

46

Acronyms

ASU – Asymmetric unit
TULIP – Tubular lipid binding protein
SMP – Synaptotagmin-like mitochondrial-lipid-binding protein
LPT – Lipopolysaccharide transport
MLA - Maintenance of OM lipid asymmetry
BPI – Bacterial permeability-increasing protein
CETP – Cholesteryl ester transfer protein
LBP – LPS-binding protein
E-Syt – Extended Syntaptotagmin
ERMES – ER mitochondrial encounter structure
RMSD – Root mean square deviation
TLC – Thin layer chromatography
ITC – Isothermal titration calorimetry
QCM-D – Quartz crystal microbalance with dissipation
PDB – protein data bank
CL – cardiolipin
PE – Phosphatidylethanolamine
PG – phosphatidylglycerol
AFDB50 – AlphaFold Database 50

Introduction

Bdellovibrio bacteriovorus is a predatory bacterium that preys on other Gram-negative bacteria. Upon prey encounter, *B. bacteriovorus* attaches to its prey and invades its periplasm, where it remodels the host peptidoglycan to form a rounded bdelloplast. Here, it liberates prey biomolecules for its filamentous growth, followed by septation into progeny. Finally, when the prey cell is exhausted of nutrients, it becomes lysed to release free swimming *B. bacteriovorus* to repeat the cycle anew [1]. This remarkable prey-killing lifestyle, and its indifference to prey antibiotic-resistance status gives *Bdellovibrio* huge potential as a novel biological control agent [2]. However, this lifestyle also requires a wealth of specialised tools [3]. Indeed, *Bdellovibrio* utilizes a number of liberated biomolecules from its prey [4-7],

including both lipid A [8] and fatty acids [9]. These lipids can either remain in their original form or undergo metabolic alterations by *Bdellovibrio*.

Bdellovibrio's intricate association with membranes is central to its predatory lifestyle. Membrane and cell wall remodelling [10-12], as well as lipid uptake [8, 9] are critical facets of host cell penetration and subsequent intraperiplasmic survival. The mechanisms through which *Bdellovibrio* obtains lipids from its prey remain elusive, highlighting the complexity of lipid transport in bacteria, which typically necessitates dedicated machinery, such as the Lpt or Mla systems for lipid movement across the aqueous periplasmic environment [13]. However, these systems are responsible for intracellular transport of lipids across the periplasm of a cell, shuttling between inner and outer membranes. *Bdellovibrio* has the additional need for intercellular lipid transport, to extract and transfer lipids from prey cell membranes to self.

Tubular lipid-binding proteins (TULIPs) exhibit unique structural features comprising a cylindrical fold that surrounds a hydrophobic cavity, enabling them to sequester lipids from the surrounding environment. These include the extracellular bacterial permeability increasing protein-like (BPI-like) double-TULIP family, Takeout-like proteins and intracellular Synaptotagmin-like mitochondrial-lipid-binding protein (SMP) family [14, 15]. TULIPs have gained attention for their diverse roles in membrane tethering, lipid transfer, hormone binding and innate immunity in eukaryotes [15, 16]. Recently, widespread identification in prokaryotes has made it clear that TULIPs have important roles in prokaryote physiology [17, 18]. Structurally characterised prokaryotic TULIPS are few, and include *E. coli* YceB, and *Clostridium botulinum* neurotoxins/neurotoxin-associated proteins, P47 and OrfX proteins [19, 20]. Understanding the molecular mechanisms governing TULIP-lipid interactions is crucial for deciphering their role in prokaryotic organisms, inclusive of alternative lifestyles like the predator *Bdellovibrio*.

In this study, we provide X-ray crystal structures of two proteins encoded from the operonal gene cluster *bd2538* and *bd2539,* TULIP invasion protein A (TipA) and TULIP-associated invasion protein B (TipB), respectively. These proteins are upregulated during the invasion process [21] and secreted into prey [22]. We show that TipA forms a novel dimeric BPI-like double-TULIP, longer than classical characterized family representatives, and that TipB binds to TipA to induce a conformational opening of the TULIP fold. These results provide the first

113 example of a lipid-binding protein in *Bdellovibrio* and provide insight into the molecular
114 mechanisms of lipid trafficking during its predatory lifestyle.
115
116 **Results**
117
118 **Bdellovibrio TipA is a BPI-like double TULIP divergent from other family**
119 **members**
120
121 The operonal genes *bd2538* and *bd2539* (Fig. 1A) encode two proteins we term TULIP
122 invasion protein A (TipA) and TULIP-associated invasion protein B (TipB), respectively. To
123 identify the role of TipA in predation we sought to determine its structure (mature enzyme,
124 minus signal peptide) and elucidate its function. The crystal structure of selenomethionine-
125 incorporated TipA was solved in space group P 3_1 2 at 4 Å resolution with three molecules in
126 the asymmetric unit (ASU). The low resolution of diffraction was likely a consequence of the
127 87% solvent content caused by the end-to-end packing of the proteins in the unit cell.
128 Nevertheless, maps of sufficient quality were obtained (Fig. 1B) and in all three chains, at least
129 residues N35-A566 were traced with no unmodelled gaps in the model (Fig. 1C). TipA was
130 annotated to contain a DUF2785 domain, however the crystal structure confirms mis-
131 annotation, as the protein fold shows it to be of the lipid binding protein BPI/LBP superfamily
132 (IPR030675) [23].
133
134 TipA shows similar gross features to those of other BPI/LBP family structures: a double-
135 TULIP fold, comprising a central beta sheet sandwiched by two tubular domains each formed
136 by a beta sheet that wraps around an extended helix (Fig. 1C). Each TULIP domain has the
137 typical secondary structure characteristic of that domain: an N-terminal helix (helix A), an
138 elongated beta sheet, and a C-terminal helix (helix B). The single protomer forms a cylindrical
139 protein with dimensions of approximately 142 x 35 x 40 Å enveloping a central hydrophobic
140 cavity throughout the entire protein.
141
142 TipA was submitted to the DALI server [24] to identify proteins with similar structures. The
143 top hits were all double TULIP proteins: Bacterial permeability-increasing protein (BPI; Z-
144 score 16.5; 21% seq ID), Cholesteryl ester transfer protein (CETP; Z-scores 13.5-15) and LPS-
145 binding protein (LBP; Z-scores 10.4-11). Superposition of the individual N- and C-terminal

146 domains of TipA with those of BPI shows significant divergence of the protein fold, with
147 RMSD values of 5.7 Å over 176 residues for the N-terminal domain and 5.8 Å over 112
148 residues for the C-terminal domain (Fig. 1D-E). Hence, we conclude that TipA is a divergent
149 TULIP representing a grouping of the superfamily previously uncharacterised.
150
151 The N-terminal domain shows three inserts relative to that of BPI: a beta hairpin between the
152 last beta strand and helix B, a loop containing an additional helix between the first and second
153 strands, and a small helix between the second and third strands (Fig. 1D). The first two of these
154 inserts comprise the dimerisation interface of TipA, whereas the function of the latter is
155 unclear.
156
157 Compared to BPI, the C-terminal domain has a truncated loop between strands 1 and 2, a larger
158 triangular-shaped loop between strands 2 and 3, and two small helices inserted between the last
159 strand and helix B. Superposition reveals that the central beta sheet and helix A align well with
160 the BPI C-terminal domain, but upon exit from helix A, TipA diverges greatly (Fig. 1E). In
161 particular, both the sheet and helix B are much shorter than BPI, and this causes a relative
162 displacement.
163

164 **TipA forms a cylindrical homodimer**

165
166 A surprising finding of the crystal structure of TipA was that unlike any other characterised
167 TULIP, TipA forms a C2 symmetrical dimer (Fig. 2A), with one complete dimer in the ASU
168 and one protein forming a dimer with a symmetry copy. TipA has a novel beta hairpin and
169 helix on the N-terminal domain that form a dimer interface, producing an extended
170 hydrophobic tube through an end-on-end interaction (Fig. 2A-B). The channel throughout
171 dimeric TipA is almost continuous, containing a pinch point in each of the central sheet
172 domains, and has a total volume of approximately 25000 $Å^3$ as calculated by 3vee [25] (Fig.
173 2B). The dimerisation hairpins form a single antiparallel beta sheet and produce hydrophobic
174 and polar faces with two intermolecular electrostatic interactions formed by E251 and K256
175 (Fig. 2C). A sequence alignment of TipA shows a number of highly conserved residues that
176 are important structurally (Fig. EV1). The tip of the dimerisation hairpin contains a highly
177 conserved asparagine (N253) that hydrogen bonds with the backbone of F184. N260 is also
178 highly conserved and serves to propagate helix B following the hairpin. The highly conserved

179 P246 kinks the backbone to bend the hairpin away from the beta sheet and angle it parallel to
180 the protein tube, allowing interdigitation with the hairpin of the second molecule. The N-
181 terminus of the dimerisation helix packs against its own helix B and extends outwards to pack
182 its C-terminal tryptophan into the hydrophobic face of the other protomer's helix B (Fig. 2D).
183 The dimerisation helix makes hydrogen bonds between Q104 and Q104, and E263 and Q111.
184 The associated loop (L113-S117) forms backbone hydrophobic interactions through L113 and
185 F116 and backbone hydrogen bonds between V114 and Y258. A highly conserved glycine
186 (G115) allows the chain to form a sharp turn to thread back to the beta sheet of the N-terminal
187 domain.
188
189 Due to the spacious packing of the TipA dimer crystals, and consequent relatively low
190 resolution, we subsequently sought to obtain a higher resolution structure of TipA by altering
191 the packing of the crystal lattice. To do this we substituted the hairpin region (A249-F258) with
192 a triple glycine linker, termed $TipA_{\Delta Hairpin}$. We expected the loss of dimerisation to allow better
193 packing of the protein, reducing solvent content to produce higher resolution diffraction. This
194 substitution shifted the elution volume of the protein from 164 mL to 200 mL on a Superdex
195 200 pg 26/60 column, showing a drastic decrease in hydrodynamic radius of the protein, and
196 indicating that the protein is primarily monomeric in solution (Fig. 2E). As predicted, the
197 $TipA_{\Delta Hairpin}$ protein crystallised with different packing in space group P 2_1 2_1 2_1, with a solvent
198 content of 60% and higher resolution diffraction of 2.6 Å. The crystal structure of $TipA_{\Delta Hairpin}$
199 contains a single monomeric copy in the ASU (Fig. 2F). The lack of dimer interface introduced
200 disorder into the N-terminal domain and the regions of G107-M118 and the glycine linker
201 region P246-N253 (N260 in wild-type (WT)) so these residues could not be modelled. The C-
202 terminal domain and central sheet are very similar to that of the WT protein, but the N-terminal
203 TULIP sheet is pulled inward, mediated by a bend in Helix B at G277 (G284 in WT). This
204 suggests that dimerisation is integral to maintaining correct folding of the N-terminal domain.
205

206 **TULIP partner TipB is a β-sandwich with exposed hydrophobic loops**

207 Since the TipA-encoding *bd2538* gene is in a predicted operon with the downstream *bd2539*
208 gene, which it overlaps by 4 nucleotides and which we name *tipB*, we hypothesised that TipB
209 could be functionally linked to TipA. Following our structural studies of TipA, we purified and
210 crystalized the cryptic operonal TipB protein. TipB crystallised in space group C 2 2 2_1 with
211 three copies in the ASU and diffracted to 2.17 Å resolution. The structure reveals that TipB

212 forms a compact β-sandwich, in which one four-strand anti-parallel sheet forms the central
213 globular core of the protein and is packed on one side by a pair of short beta sheets and the
214 other side by an elongated capping-loop extending from β7 and β8 (Fig. 3A). This loop folds
215 back on the sheet burying Y120, W122 and M133 into the core. The protein has another pair
216 of loops that extend between β3 and β4, and β6 and β7, termed interaction loops 1 and 2,
217 respectively (Fig. 3A). Importantly, both loops have hydrophobic residues at the ends: F65 and
218 I66 in loop 1 and F103 in loop 2, and demonstrate a high degree of flexibility (as inferred by
219 electron density and B-factor values; Fig 3B). Finally, the protein contains a short helical turn
220 between strands 2 and 3 and an 11-residue helix between strands 8 and 9.

221 We used the DALI server [24] to identify structural homologues of TipB and the highest
222 scoring structure was *P. aeruginosa* ExsB [26] (PDB code 2YJL), with a Z-score of 7.3. Both
223 TipB and ExsB show a topology similar to that of type II C2 domains (Fig. 3C-E) [27], a
224 calcium-dependent membrane-localisation domain found in multiple eukaryotic signalling
225 proteins including kinases [28], lipases [29] and membrane trafficking proteins [30]. In
226 comparison, TipB lacks the 8th strand that runs antiparallel between the 1st and 7th strands,
227 instead packing its last strand parallel to the 2nd strand (the 1st strand is broken into two smaller
228 strands due to a broken beta sheet in TipB), forming a mixed sheet. The other top-scoring hits
229 all had the standard type II C2-domain topology, with varying additional loops and secondary
230 structure components. Most of the C2-domain proteins have an exposed face on the beta sheet,
231 however some homologues show extensions in the β7 and β8 loop that cap off this sheet in a
232 similar manner to TipB (Fig. 3E). None of the homologues had extensions between β3 and β4
233 or β6 and β7 strands where the interaction loops are observed in TipB.

234 ExsB has an exposed beta sheet with a basic face predicted to mediate binding to acidic lipids
235 (Fig. 3E). In TipB, this sheet face is not exposed and forms part of the hydrophobic core that
236 is enclosed by an extended loop between β7 and β8. To investigate whether TipB would adhere
237 to a lipid bilayer, we used quartz crystal microbalance with dissipation monitoring (QCM-D)
238 measurements (Fig. 3F). This surface-based technique monitors changes to the resonant
239 frequency of a surface (Δf) under an applied voltage. Δf is inversely proportional to the mass
240 deposited on the surface, and as such allows us to monitor interactions between biomolecules
241 [31]. In the case of TipB-lipid interactions, a stable POPC bilayer was deposited onto a silicon
242 QCM-D sensor, following well-established methods [32, 33]. Despite not being a constituent
243 of bacterial membranes, a POPC bilayer was used here due to its well-reported ability to form

244 highly stable bilayers when deposited onto a surface [34]. Once lipid bilayers were deposited,
245 TipB was introduced and its interaction with the lipid bilayer was assessed in a semi-
246 quantitative manner. Upon flow of TipB over the bilayer, negligible frequency (0.3 Hz) and
247 dissipation (0.48 ppm) changes occurred, thus confirming that TipB alone does not bind
248 directly to lipid membranes.

249

250 C2 domains commonly bind calcium, such as the high-scoring DALI hit *Homo sapiens*
251 phospholipase 2 [35]. We wanted to confirm that TipB doesn't bind calcium as it does not
252 contain obvious calcium-binding residues nor was calcium observed in the crystal structure.
253 After treatment with 5 mM EGTA and 5 mM EDTA, and subsequent gel filtration, no binding
254 was seen using isothermal titration calorimetry (ITC; Fig. 3G), confirming that TipB is a
255 calcium-independent C2-like β-sandwich.

256

257 **TipA and TipB form a TULIP:partner complex**

258

259 Since TipB did not display any phospholipid binding activity we next hypothesised that TipA
260 and TipB might interact with each other in a functional manner (whilst also being stable in their
261 isolated states, as inferred from our structures). Isothermal titration calorimetry (ITC) of TipB
262 into TipA resulted in a clear binding curve (Fig. 4A), and the -TΔS value suggests the
263 interaction is largely driven through entropy effects, possibly through hydrophobic
264 contributions. However, due to the low stoichiometry observed (0.25), the curve wasn't
265 suitable to calculate an accurate Kd. The relatively poor stability of the TipA protein would not
266 allow for higher concentrations to be used. The low stoichiometry could result from TipA
267 existing as multiple species in solution. Although TipA elutes as a single peak in gel filtration
268 experiments, this peak is broad (when compared with ΔHairpin TipA), potentially the result of
269 multiple TipA conformers (Fig. 2E). It is therefore likely that only a subpopulation of TipA is
270 competent for binding and may further demonstrate the flexible nature of the protein.

271

272 We subsequently desired to obtain a crystal structure of the complex of TipA and TipB. The
273 two proteins were purified and mixed with a molar excess of TipB in the crystallisation
274 conditions in order to ensure a complex of the two proteins. This complex crystallised in space
275 group P 2 2 2_1 and diffracted to 2.6 Å with one copy of each protein in the ASU. The TipA
276 component formed a dimer on a crystallographic 2-fold axis exhibiting the same hairpin-helix

277 dimer interface as the selenomethionine-labelled TipA crystals (Fig. 4B). TipB can be observed
278 binding centrally on TipA, straddling the unusually kinked helix A, which protrudes away from
279 the beta sheet, forming a triangular seat (Fig. 4C-E). The structure of complexed TipB is very
280 similar to that of TipB alone, with RMSDs ranging from 1.43 to 1.81 Å over 139 amino acids
281 for the three chains of the TipB crystal structure. Differences are mostly observed in interaction
282 loops 1 and 2, which fold down over the seat and bury residues F65, I66 and F103 into the
283 hydrophobic lumen of TipA (Fig. 4F-G). In addition to the hydrophobic components, there are
284 a number of hydrogen and electrostatic bonds from side chains and backbone atoms throughout
285 the 1346 $Å^2$ interface (Fig. 4H-I), as calculated by PISA [36].
286

287 **Partner TipB binds to open up the TULIP fold and central cavity**

288

289 The most striking observation of the complex structure is the conformational change seen in
290 TipA's N-terminal domain (Fig. 5A-B). While the superposition of the C-terminal domains of
291 the apo and complexed TipA structures show an RMSD of 1.26 Å over 261 residues, the N-
292 terminal domain shows an RMSD of 6.13 Å over 271 residues. The N-terminal domain of the
293 TipA apo structure comprises an almost completely closed tube, with very little access to
294 solvent (Fig. 5C). However, the N-terminal domain of the complex is in an open conformation,
295 with a gap of approximately 20 Å (from Y80-S282; Fig. 5D). This opening is mediated by an
296 approximate 45° rotation of the protruding TipA helix A (Fig. 5A), which acts like a lever,
297 pulling the N-terminal sheet open. This opening is also stabilised by the anchoring of
298 interaction loop 1 into the C-terminal domain, and the packing of interaction loop 2 F103 under
299 the lifted N-terminal sheet. TipB F103 acts as a clamp underneath the TipA beta sheet in
300 concert with K100 and R34, which form electrostatic interactions with E72 and E129,
301 respectively, on the top of the sheet (Fig. 5E). Analysis by DynDom [37] characterises this as
302 a hinge mechanism, comprising three moving domains (Fig 5F): the C-terminal domain and
303 most of the N-terminal helix B (Domain 1); most of the N-terminal sheet and dimerisation
304 hairpin (Domain 2); and the end of the N-terminal sheet and dimerisation helix (Domain 3).
305 The analysis identifies two hinge points between these domains which include the rotation
306 point of the N-terminal helix A seat. Domain 2 rotates approximately 29° relative to Domain 1
307 and Domain 3 rotates 36° relative to Domain 2, keeping it a similar relative position to Domain
308 1 in both structures (Fig. 5G). Hence, the function of TipB is to convert TipA to a more open
309 form and, to the best of our knowledge, represents a new type of TULIP binding-partner.

310

311 Using Foldseek [38] to search for homologous proteins, we observe double-TULIPs with
312 additional fused domains (Fig. EV2). These include beta-rich domains, helical bundles and
313 mixed domains including enzymes and entire double-TULIP repeats. Of particular interest is
314 the presence of a double-TULIP in the *Planctomyces sp*. SH-PL14 protein, Uniprot accession
315 A0A142WTQ2. This protein contains a fused N-terminal esterase-like enzyme in addition to a
316 C-terminal beta-sandwich. This beta-sandwich has similar topology to TipB, and is also
317 predicted to localise on the N-terminal Helix A and sheet, suggesting that it could have a similar
318 role to TipB in this system.

319

320 **TipA binds rapidly to membrane bilayer surfaces**

321

322 During the purification process of TipA, we observed that under conventional buffer conditions
323 (<500 mM NaCl) the protein remained largely in the pellet after lysis and centrifugation.
324 However, upon addition of high salt concentrations or detergents, the protein was released into
325 the supernatant. This led us to believe that the protein was adhering to the membrane fraction
326 (Fig. 6A).

327

328 To confirm this, we again used QCM-D (Fig. 6B-E). To investigate TipA-lipid interactions,
329 stable bilayers consisting of either *E. coli* polar lipids, POPC or mixed POPC:LPS lipids were
330 deposited onto a silicon QCM-D sensor. Upon introduction of TipA to all three bilayer
331 compositions monitored here, it exerted a dramatic negative Δf, suggesting it was rapidly
332 deposited into the bilayer systems. This interaction was most pronounced for TipA deposition
333 into POPC:LPS bilayers (Fig. 6D), with a Δf3 of -1106 Hz, compared to -1064 Hz and -686
334 Hz for POPC and polar lipid bilayers, respectively. In all bilayers tested, a critical point was
335 reached upon which further addition of TipA resulted in removal of mass from the surface.
336 This suggests an ability to first insert into lipid bilayers followed by membrane disruption.
337 Furthermore, in bilayers containing POPC a double-dip insertion of TULIP was observed (Fig.
338 6C-D), which may result from the ability of POPC to form more stable bilayers on silicon
339 surfaces than *E. coli* polar lipids. Interestingly, this distinctive mode of interaction was not
340 observed when TipA was introduced to an empty silicon surface generated through the inability
341 to deposit polar lipid:LPS bilayers, with no major mass deposition or removal observed (Fig.
342 6E).

343

344 **Lipids are observed in the TipA TULIP lumen in multiple states**

345

346 In order to confirm that TipA is a classic TULIP that binds lipids within its cavity, thin layer
347 chromatography (TLC) was performed (Fig. 7A). TipA clearly copurifies with all three
348 common *E. coli* polar lipids, cardiolipin (CL), phosphatidylethanolamine (PE) and
349 phosphatidylglycerol (PG). These have likely been extracted from *E. coli* during the expression
350 or extraction process. Density for lipids was observed in all three crystal structures, however
351 the low resolution of the selenomethionine form prevented their modelling (Fig. EV2A). In
352 both the 2.6 Å TipAB complex structure (Fig. 7B) and the 2.6 Å monomeric $TipA_{\Delta Hairpin}$
353 structure (Fig. 7C), clear densities are observed for two lipid head groups in the N-terminal
354 TULIP domain. It was also possible to trace the lipid tails in the $TipA_{\Delta Hairpin}$ structure but not
355 in the complex structure. The lipids were modelled as PE as this headgroup fit the density well
356 (Fig. 7D), and the density would not accommodate the glycerol moiety of PG, nor did the
357 density indicate the presence of the double headgroup of CL.

358

359 In both structures the lipid headgroups are seen in similar regions in the protein (as are the Fo-
360 Fc peaks in the selenomethionine TipA structure; Fig. EV2A), one underneath Helix A, and
361 the other between the sheet and Helix B (Fig. 7E-F). However, contributing amino acids that
362 bind the ligand are different between the structures. The placement of the inner lipid in the
363 TipAB structure means that the headgroup makes a H-bond and hydrophobic interactions with
364 G102 and F103. In the $TipA_{\Delta Hairpin}$ structure (where TipB is not present), it makes H-bonds
365 with Y132 and K69, but additional interactions are formed by V493 of the symmetry copy,
366 providing a backbone H-bond and sidechain hydrophobic interactions. These modelling
367 differences suggest that TipB affects lipid interactions with TipA.

368

369 Interestingly, in both structures one of the lipids makes contact with the C-terminal domain of
370 a symmetry copy (Fig. EV2B-D), with polar contributions from the symmetry copy K457 and
371 K503 to the phosphate moiety of the outer lipid in the TipAB structure. When visualising
372 higher order packing in all three TipA structures, this is a common occurrence – in three
373 different space groups the C-terminal hydrophobic residues M454, F455, L504 and F505 pack
374 into the N-terminal domain 'seam' between Helix B and the 1st beta strand (Fig. EV2E-G).

375 Further structures of close TipA homologues are needed to determine if this mode of interaction
376 is a conserved feature.
377

378 **Discussion**

379 Tubular lipid binding proteins (TULIP) proteins are a universal lipid-binding fold,
380 characterised by their ability to sequester lipids within their internal hydrophobic cavities.
381 Whilst these folds are ubiquitous to all domains of life, prokaryotic TULIPS present an under-
382 represented group within the literature [17]. We have structurally characterised the first
383 example of a lipid-binding protein from *Bdellovibrio bacteriovorus* HD100 - the predation-
384 associated TULIP, TipA, and identified an associated adapter protein TipB.
385

386 TipA is in the same superfamily as the eukaryotic bacterial permeability increasing protein
387 (BPI), which also forms a double-TULIP fold. The protein shows similar structural features to
388 that of other BPI-like proteins, such as the classical Helix-ββββ-Helix TULIP core secondary
389 structure, two TULIP domains back-to-back with an intervening central sheet, and longer N-
390 terminal than C-terminal TULIP domain. However, modifications to the protein have made the
391 overall fold divergent, with the addition of molecular features that enable the formation of a
392 dimeric double-TULIP, and for interaction with the TipB adapter protein. The dimerisation
393 motif includes an additional hairpin and helix that lock the homodimer together to form a
394 hugely elongated ~260 Å tube.
395

396 While no other double-TULIP has been observed in a dimeric form, the extended
397 synaptotagmins (E-Syts) and the eukaryotic ER-mitochondria encounter structure (ERMES)
398 proteins do form single-TULIP homodimers, but they pack using a different interface where
399 helix B packs against the beta sheet edge [39]. It is interesting that a heterotetrameric form of
400 TULIP is also seen between ERMES proteins Mdm12 and Mmm1, where heterodimers stack
401 head-to-head through an Mmm1-Mmm1 interface [40]. This creates an equivalent chain of four
402 TULIP domains, highlighting that higher-order arrangements of TULIPs are functionally
403 significant. It is possible that this increase in TULIP length is needed in order to efficiently
404 transport lipids effectively at some juncture between prey and *Bdellovibrio*. The length of the
405 dimer is between 250 and 260 Å which is equivalent to that of the periplasmic spanning
406 transporter complexes, Yeb and Pqi [41] as well as the predicted structure of the putative
407 transporter YhdP [42]. ERMES proteins and E-Syts tether membranes and transfer lipids

408 between them, which is dependent on the presence of their C2 domains for membrane tethering
409 [43], and therefore proximity of membranes to their single-TULIP is required. The increased
410 length of the TipA dimer could allow for lipid transfer between membranes without the need
411 for direct membrane tethering by additional domains.
412
413 It is also noteworthy that we consistently observe TipA packing C-terminal hydrophobic
414 residues into the N-terminal domain – which creates a network of TULIPs in the crystal lattice.
415 This could indicate that during predation TipA could form higher order structures that facilitate
416 transport of lipids from TULIP to TULIP. Higher order structures also occur in the ERMES
417 complex as the Mmm1-Mdm12 complex also interacts with another TULIP Mdm34 [40, 44],
418 but structural information and exact stoichiometry is unknown for these larger complexes.
419 Further work could confirm whether there is a physiological function for this consistent C-
420 terminal-N-terminal TULIP packing of TipA.
421
422 The *tipA* gene is in an operon with *tipB*, which encodes for a small C2-like sandwich domain.
423 The functional link between TULIPs and C2 domains is observed in ERMES and E-Syt
424 systems, where the C2 domains mediate membrane tethering. TipB, while C2-like, does not
425 bind calcium or membranes, and functions in an entirely different manner. The TipB sandwich
426 has been adorned with two extended loops that are used for interaction with TipA by insertion
427 into its lumen. The crystal structure of the complex of TipA and TipB shows that upon binding
428 of the two proteins there is a large conformational change in TipA, mediated by a clamping
429 mechanism that lifts its N-terminal beta sheet. This creates an opening of the TULIP seam,
430 creating an accessible core across both N-terminal domains of the TipA dimer. Previously, a
431 gate-and-latch mechanism has been proposed to account for lipid binding into the lumen of the
432 single-TULIP juvenile-hormone binding protein from the domestic silk moth [45]. Here, the
433 N-terminal helix A opens in the apo form and closes on the buried sesquiterpene molecule
434 when bound. As the N-terminal helix of double-TULIP proteins is locked into the central beta
435 sheet by an additional N-terminal beta strand, this latch mechanism is not possible. Instead, it
436 is possible that the opening of TipA by TipB is what facilitates loading or unloading of lipids;
437 observation of lipid-loaded recombinant TipA by TLC indicates that it would not be dependent
438 on TipB. The intriguing finding of a planctomycete double-TULIP with a fused beta-sandwich
439 that binds to the N-terminal domain Helix A and sheet proposes the idea that this functional
440 relationship is repeated across diverse bacteria. In addition, it is possible that TipA
441 homodimerisation is also required to ensure the stability of the overall fold during this opening

442 and closing process as we have observed a high degree of flexibility in the N-terminal sheet
443 (very pronounced in TipA$_{\Delta hairpin}$), and the lumen of the N-terminal domain is larger than
444 typically observed in other double-TULIPs.
445
446 We were unsuccessful in attempts to monitor TipA localisation – trials with a C-terminal
447 mCherry tag resulted in frequent mutational escape, so TipA could not be investigated by
448 fluorescence microscopy; future studies could use antibodies or computational-design binders
449 to address this issue. TipA's ability to adhere to membranes and destabilise them as shown via
450 QCM-D suggests that it could be used to extract lipids directly from prey bacterial membranes.
451 Binding and membrane destabilisation by TipA could aid *Bdellovibrio*, and could work in a
452 similar fashion to BPI [46] by increasing membrane permeability. TipA is not the first example
453 of a TULIP protein adhering to membranes without C2 domain partners - tricalbin 2 (a yeast
454 E-syt homologue) and nucleus-vacuole junction protein 1 TULIP domains were shown to bind
455 to membranes *in vitro* using liposomes [47], and the tricalbins are known to transfer lipids
456 between membrane contact sites. Therefore, membrane adherence (as observed by both our
457 purification procedure and QCM-D experiments) is likely an effective way for TipA to uptake
458 lipids into its core ready for transfer to another protein or membrane.
459
460 In conclusion, our findings underscore the evolutionary significance of TULIPs as universal
461 lipid-binding folds across both eukaryotes and prokaryotes. The crystal structures of TipA,
462 TipB and their binary complex show that *B. bacteriovorus* has novel lipid-binding machinery
463 for its predatory lifestyle in the form of a modified dimeric double-TULIP protein. Through
464 the mechanistic interdependence of TipA and TipB, we give new insight into the
465 conformational changes possible in double-TULIP proteins and suggest an adaptor-mediated
466 mechanism for promoting lipid loading and unloading.
467

468 **Methods**

469

470 **Cloning, expression and purification**

471

472 TipA-His was cloned into a modified version of the pET41c overexpression vector using
473 restriction-free cloning methods. The final construct contained residues of 26-572 of TipA
474 (Uniprot accession Q6MK73) fused to a C-terminal octa-His-tag. TipB was cloned into pET26b

475 using NdeI and NotI. A tagless form of TipA was made by mutagenesis to remove the octa-
476 Histag. A monomeric form of tagless TipA ($TipA_{\Delta Hairpin}$) was created using Q5 mutagenesis,
477 replacing the dimer-hairpin residues A249-Y-258 (AVEVNGKKFY) with a triple glycine
478 linker. TipB was cloned into pET26b using NdeI and XhoI restriction sites. The final construct
479 contained an N-terminal MAHHHHHH tag and residues 29-171 of TipB (Uniprot accession
480 Q6MK72).
481
482 To express selenomethionine-labelled TipA, a 60 mL overnight culture of BL21 (DE3) cells in
483 LB was centrifuged and resuspended in minimal media supplemented with kanamycin and
484 chloramphenicol to a final volume of 1 L. At OD_{600} 0.4, 0.1 g of lysine, 0.1 g of threonine, 0.1
485 g of phenylalanine, 0.05 g leucine, 0.05 g of isoleucine, 0.05 g of valine and 0.06 g of
486 selenomethionine were added to the culture. After 15 minutes, IPTG was added to 1 mM. Cells
487 were harvested by centrifugation after 16 h at 18 ˚C and stored at -20 ˚C.
488
489 $TipA_{\Delta Hairpin}$, TipA-His and TipB constructs were expressed in *Escherichia coli* BL21 RIPL
490 (DE3). Cells were grown in LB supplemented with kanamycin to an OD_{600} of 0.5-0.7 and
491 induced with 0.5 mM IPTG at 18 °C for 16 h. Cells were harvested by centrifugation at 4000g
492 for 15 minutes. During trial purifications we noted that the majority of TipA protein sedimented
493 with insoluble cell components following lysis and centrifugation, but could be liberated from
494 the insoluble pellet by the addition of high (1M) NaCl. We exploited this characteristic of TipA
495 in our subsequent purification protocols. Cells expressing untagged selenomethionine-labelled
496 TipA and $TipA_{\Delta Hairpin}$ were resuspended in wash buffer (50 mM HEPES and 0.15 M NaCl, pH
497 7.5), sonicated and centrifuged at 48384 g for 1 h. The pellet was again resuspended, sonicated
498 and centrifuged to wash away soluble proteins. A third pellet wash was performed and finally
499 the pellet was resuspended in 50 mM HEPES and 1 M NaCl, pH 7.5. Cells expressing his-
500 tagged proteins were resuspended in buffer A (TipA-His - 50 mM HEPES and 1M NaCl, pH
501 7.5; TipB - 50 mM HEPES and 300 mM NaCl, pH 7.5). The cells were lysed by sonication on
502 ice and centrifuged at 48384 g for 1 hour. The pellet was resuspended. The lysates were loaded
503 onto a 5 mL Ni-NTA column (GE Healthcare) and washed with 10 CV of lysis buffer. The
504 protein was eluted with a gradient of 20–500 mM imidazole. All proteins were finally passed
505 through a Superdex 200 pg or 75 pg 26/60 column (GE Healthcare), which was pre-equilibrated
506 with 20 mM HEPES, 150 mM NaCl, pH 7.5. Fractions containing the protein of interest were
507 pooled, concentrated and stored frozen at -70 °C if not required for immediate use.
508

509 **Crystallisation**

510

511 Selenomethionine-lebelled TipA crystallisation screens were prepared by mixing a 1.5 µL of 8
512 mg/mL TipA and 1.5 µL precipitant solution. TipA crystallised in space group P 31 2 1 (a
513 =252.4, b=252.4, c=181.1, α=90, β=90, γ=120) in a precipitant solution from the Jena
514 Bioscience JBS Classic Screen consisting of 15% w/v PEG 4000; 100 mM trisosodium citrate,
515 pH 5.6; 200 mM ammonium sulphate. Diffraction data were collected at Diamond Light
516 Source. Data reduction and processing were performed using XDS.

517

518 $TipA_{\Delta Hairpin}$ crystallisation screens were prepared by mixing a 0.4 µL of 10 mg/mL TipA and
519 0.4 µL precipitant solution. TipA crystallised in space group P 21 21 21 (a =58.0, b=97.8,
520 c=132.0, α=90, β=90, γ=90) in a precipitant solution from the BCS screen consisting of 0.1 M
521 MES pH 6.5, 2% v/v PEG 400, 2% v/v PEG 500 MME, 2% v/v PEG 600, 2% w/v PEG 1000,
522 2% w/v PEG 2000, 2% w/v PEG 3350, 2% w/v PEG 4000, 2% w/v PEG 5000 MME, 2% w/v
523 PEG 6000, 2% w/v PEG 8000, 2% w/v PEG 10000. Diffraction data were collected at Diamond
524 Light Source. Data reduction and processing were performed through the Xia-2 Dials pipline,
525 and Aimless.

526

527 TipB crystallisation screens were prepared by mixing a 0.4 µL of 10 mg/mL TipB and 0.4 µL
528 precipitant solution. TipB crystallised in space group C 2 2 21 (a =106.6, b=126.2, c=78.0,
529 α=90, β=90, γ=90) in a precipitant solution from the Morpheus screen consisting of 0.03 M
530 Diethylene glycol; 0.03 M Triethylene glycol; 0.03 M Tetraethylene glycol; 0.03 M
531 Pentaethylene glycol, 0.1 M Bicine, 0.1 M Tris, pH 8.5, 20% v/v PEG 500 MME, 10 % PEG
532 20000. Diffraction data were collected at Diamond Light Source. Data reduction and
533 processing were performed through the Autoproc suite, and Aimless.

534

535 TipAB crystallisation screens were prepared by mixing a 0.5 µL of 8 mg/mL TipA and 9.5
536 mg/mL TipB (approx. 5X molar ratio) and 0.5 µL precipitant solution. The TipAB complex
537 crystallised in space group C 2 2 21 (a =89.3, b=230.7, c=131.6, α=90, β=90, γ=90) in a
538 precipitant solution from the Proplex screen consisting of 0.1 M Sodium acetate pH 5, 0 2 %
539 w/v PEG 4000 15 % v/v MPD. Diffraction data were collected at European Synchrotron
540 Radiation Facility. Data reduction and processing were performed through the Xia2-Dials
541 pipeline.

542

543 **Structure determination and model building**

544

545 Diffraction data processing and refinement statistics are given in Table EV1.

546

547 The crystal structure of Selenomethionine-labelled TipA was solved using Phenix, with manual
548 interpretation and improvement of non-crystallographic symmetry operators.

549

550 The crystal structure of TipB was solved by molecular replacement with a Colabfold model
551 [48] in Phenix MR [49] Likewise, $TipA_{\Delta hairpin}$ was solved by molecular replacement with the
552 C-terminal domain of the selenomethionine-labelled TipA and manual boot-strap building and
553 refinement of the N-terminal domain. The complex TipAB structure was solved using
554 molecular replacement of the TipB structure with the interaction loops removed, and the C-
555 terminal domain of the selenomethionine-labelled TipA structure. The N-terminal domain was
556 also manually built through boot-strap building and refinement. All structures were refined
557 through iterative cycles of real-space building in Coot [50] and refinement in Phenix Refine
558 [51].

559

560 **Pellet binding assays**

561

562 Untagged TipA was expressed in *Escherichia coli* BL21 RIPL (DE3). Cells were grown in 10
563 mL LB supplemented with kanamycin to an OD_{600} of 0.5-0.7 and induced with 0.5 mM IPTG
564 at 18 °C for 16 h. 5 X 1 mL of cells were centrifuged at 13000 RPM for 15 seconds and the
565 supernatant was removed. The cells were resuspended in 500 µL of either 0.15 M NaCl, 0.05
566 M HEPES pH 7.5; 0.5 M NaCl, 0.05 M HEPES pH 7.5; 1 M NaCl, 0.05 M HEPES pH 7.5;
567 0.15 M NaCl, 0.05 M HEPES pH 7.5, 0.05% Triton X100; 0.15 M NaCl, 0.05 M HEPES pH
568 7.5, 0.05% Tween 20. sonicated for 15 seconds and centrifuged at 13000 RPM for 15 minutes.
569 The pellet obtained from the 0.15 M NaCl buffer was resuspended in 500 µL SDS-PAGE
570 loading buffer for the pellet control. The pellet control and supernatant of each buffer was run
571 on SDS-PAGE.

572

573 **QCM-D**

574

575 QCM-D was performed using a Q-sense Analyzer QCM-D System (Biolin Scientific,
576 Gothenburg, Sweden). Silicon QCM-D sensors were fixed into the QCM-D flow cell at a
577 constant temperature of 20 °C and attached to a peristaltic pump. ddH_2O was pumped through
578 the flow cell at a constant rate of 0.1 ml/min, a rate which was subsequently maintained
579 throughout the rest of the experiment. Frequency and dissipation changes (Δf and ΔD) were
580 monitored using multiple harmonics (n = 3, 5, 7, 9, 11, 13) of the resonant frequency. For
581 simplicity we report here only the changes to the 3rd harmonic. Prior to data acquisition flow
582 cells were equilibrated in H_2O for 5 mins to allow for a stable baseline to be acquired. H2O
583 was then exchanged for buffer, which was pumped through the flow cell until the change in
584 frequency of the 3rd harmonic was stabilised. Bilayers consisting of either POPC, *E. coli* polar
585 lipids or POPC:LPS (LPS from *E. coli* O111:B4) were then deposited onto the silicon sensor.
586 This initially involves the formation of small unilamellar vesicles (SUVs), which were prepared
587 by resuspension of a desiccated POPC/E. coli Polar Lipids/POPC:LPS film in buffer in 150
588 mM NaCl, 20 mM HEPES pH 7.5 to a concentration of 0.2 mg/mL and subsequent sonication
589 for 30 min until an optically transparent solution was obtained. POPC:LPS SUVs were
590 prepared at a 10:1 (w/w) ratio. These SUVs were subsequently flowed over the silicon sensor
591 and then ruptured through osmotic shock with H2O, resulting in the characteristic formation
592 of a deposited lipid bilayer. Exchange back into buffer 150 mM NaCl, 20 mM HEPES pH 7.5
593 aids the formation of a stable bilayer, with Δf3 ranging between -35 to -45 Hz. Once bilayers
594 were deposited and baselines stabilized, TipA was introduced into the flow cell at a
595 concentration of 1 mg/ml and flowed over the deposited bilayers for ~45 mins. Excess TipA
596 was then removed by washing sensors in 150 mM NaCl, 20 mM HEPES pH 7.5. QCM-D with
597 TipB was performed as above for TipA with POPC bilayers.
598
599 An *E. coli* Polar Lipid:LPS (10:1 w/w) mixed bilayer was also attempted to be formed and
600 deposited onto silicon surfaces as outlined above. These bilayers were unable to be successfully
601 generated, with SUVs unable to rupture and subsequently washed from the sensor. These
602 surfaces were treated as 'unformed bilayers' and used as control surfaces to monitor TipA
603 interaction with empty silicon sensors.
604
605 **ITC**
606

607 To test whether TipB binds to calcium, 5 mM EDTA and 5 mM EGTA was added to the protein
608 following size exclusion. After 16 hours the protein was passed through a Superdex 75 pg
609 26/60 column (GE Healthcare), which was pre-equilibrated with 20 mM HEPES, 150 mM
610 dialysed against 1 L of 20 mM HEPES, 150 mM NaCl, pH 7.5. $CaCl_2$ was dissolved in the
611 dialysis buffer to a final concentration of 500 µM. ITC was performed by titrating 500 µM
612 $CaCl_2$ into 50 µM TipB in 13 injections (1 x 0.4, 12 x 3 µL injections).
613
614 To test whether TipB binds to TipA-His, purified protein was dialysed against 1 L of 20 mM
615 HEPES, 150 mM NaCl, pH 7.5. ITC was performed by titrating 200 µM TipB into 20 µM TipA
616 in 13 injections (1 x 0.4, 12 x 3 µL injections).
617
618
619 **TLC**
620 TLC was employed to assess the lipid binding ability of TipA. Lipids were extracted from
621 protein samples through chloroform/methanol extraction. Briefly, 2 ml of Bd2538 at 0.5 mg/ml
622 was added to 2 ml methanol and 1 ml chloroform (2:2:1, v/v/v). Samples were vortexed for 5
623 min, followed by a 30 min incubation at 50 °C and then vortexed again for 5 min.
624 Centrifugation at 2,000 x g for 10 min resulted in the formation of two phases, the lower
625 chloroform layer containing lipidic material. This lower phase was extracted and then
626 evaporated. The dried lipids were resuspended in 100 µl chloroform with 5 µl then loaded onto
627 a Silica TLC plate (Sigma) and run in a 6.5:2.5:1 (chloroform:methanol:acetic acid) solvent
628 system. The TLC plate was dried, stained with 10% (w/v) phosphomolybdic acid in ethanol,
629 and finally heated until stained spots could be visualised.
630
631
632

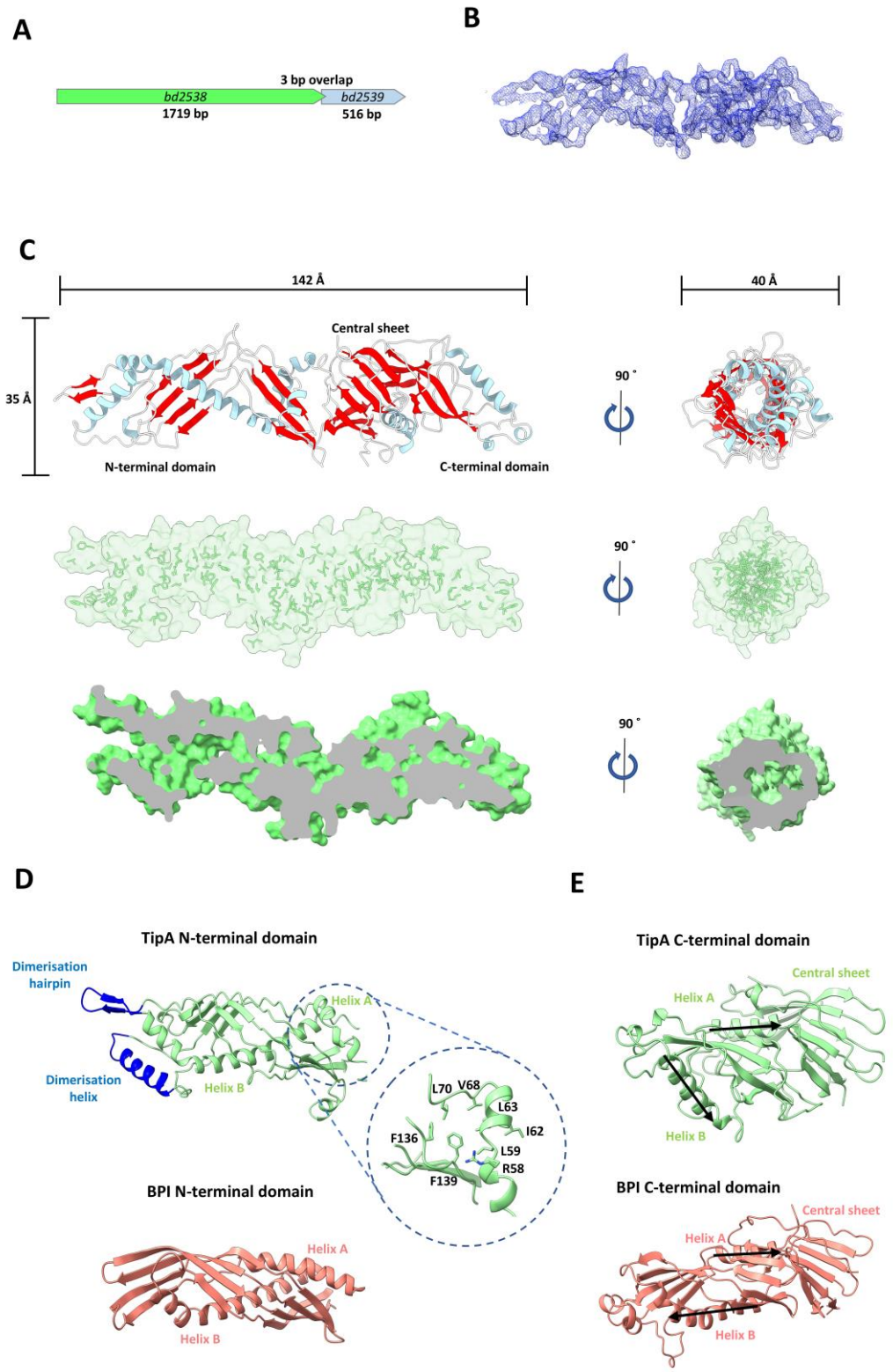

633

634 **Figure 1. The structure of *Bdellovibrio* TULIP protein TipA**

635 **(A)** Schematic of the forward strand ORFs for the gene operon of *bd2538* (green) and *bd2539* (blue). **(B)** 2Fo-Fc map at 2.5 σ surrounding
636 chain C of the crystal structure of TipA after the final refinement. **(C)** Top; Crystal structure of TipA, showing the double-TULIP fold of the
637 Bactericidal permeability-increasing protein, alpha/beta domain superfamily, coloured by secondary structure (beta – red, helix – light blue,
638 coil – white). The lengths of the protein are shown for all three dimensions. Middle; a surface view of TipA with hydrophobic residues shown

639 in stick form, highlighting the hydrophobic nature of the central cavity. Bottom; A clipped surface view showing the inner cavity. (**D)** Top;
640 structural features of the N-terminal TipA TULIP domain, with the dimerisation motif coloured blue. The expanded view shows residues in
641 stick form that cause the N-terminal Helix A to protrude. Bottom; The structure of the N-terminal TULIP domain of bacterial permeability
642 increasing protein (BPI, code 1BP1) for comparison. **(E)** Top; structural features of the C-terminal TipA TULIP domain, with the helix
643 positions highlighted with arrows. The expanded view shows residues in stick form that cause the N-terminal Helix A to protrude. Bottom;
644 The structure of the C-terminal TULIP domain of BPI for comparison.
645
646
647
648
649
650
651

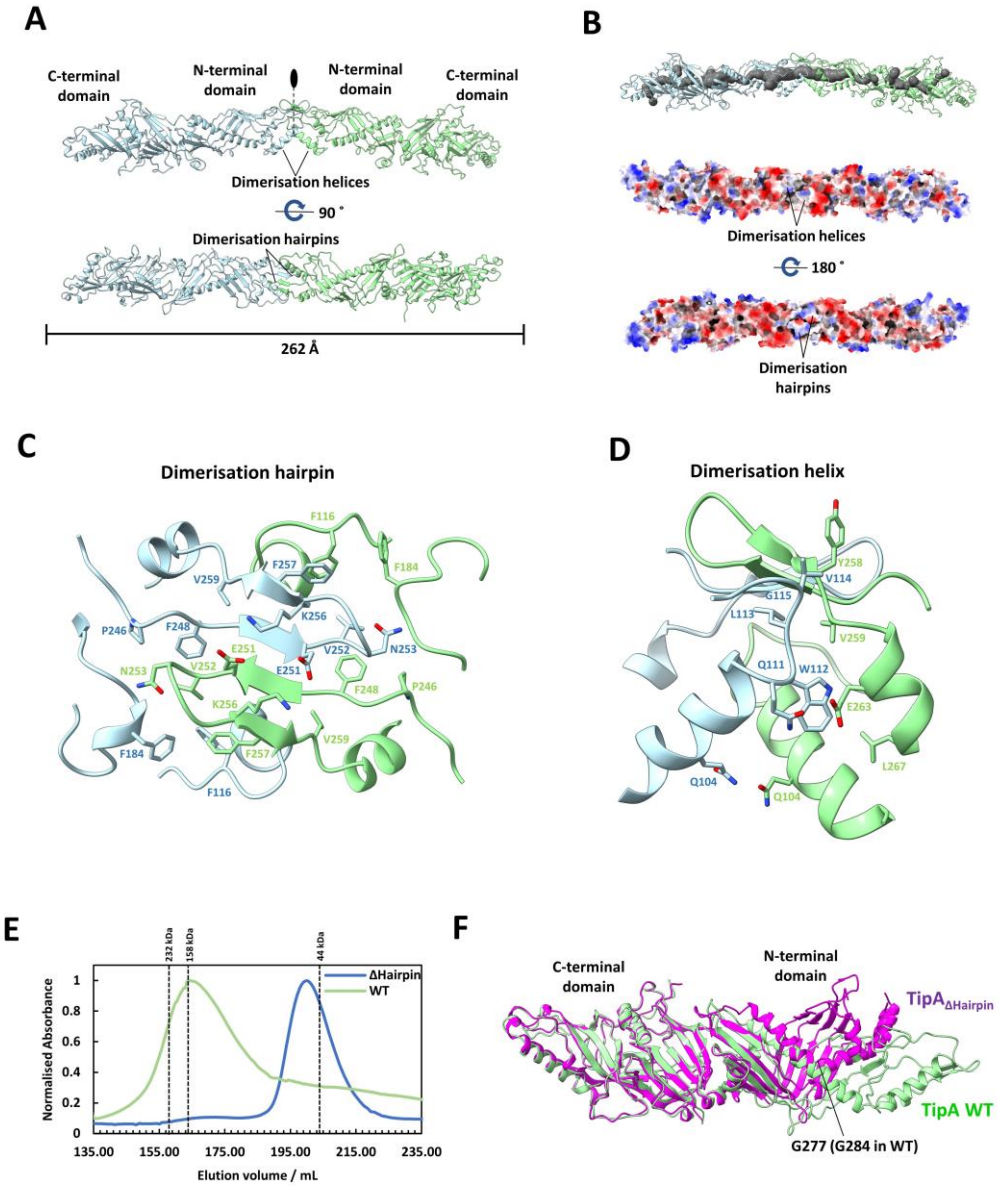

Figure 2. Dimerisation of TipA into a four TULIP-long assembly

(A) Crystal structure of TipA, showing two chains forming an end-on-end homodimer via interaction of their N-terminal TULIP domains. One protomer is shown in light blue and the other is in green with the 2-fold symmetry axis shown as a black oval and dotted line. **(B)** Upper; the dimer forms an elongated cavity within (grey surface, calculated by Mole [52]). Lower; the electrostatic surface view shows that the dimer forms a continuous tube with very few solvent accessible gaps. **(C)** The view down the two-fold axis shows how the two interdigitated dimerisation hairpins (light blue and green) create a polar surface on the outside of the TULIP dimer and a hydrophobic inner face for a continuous hydrophobic channel. **(D)** The dimerisation helix forms polar and hydrophobic interactions with the other protomer's Helix B and dimerisation helix. **(E)** Mutation of the dimerisation hairpin causes a shift in the elution volume of TipA on gel filtration from 165 mL to 200 mL. **(F)** The crystal structure of $TipA_{\Delta Hairpin}$ (magenta) superimposed onto the TipA wild type (WT) structure (green). The C-terminal domain overlays well, but the N-terminal domain is contracted due to twisting of the beta-sheet and bending of the N-terminal Helix B at G277.

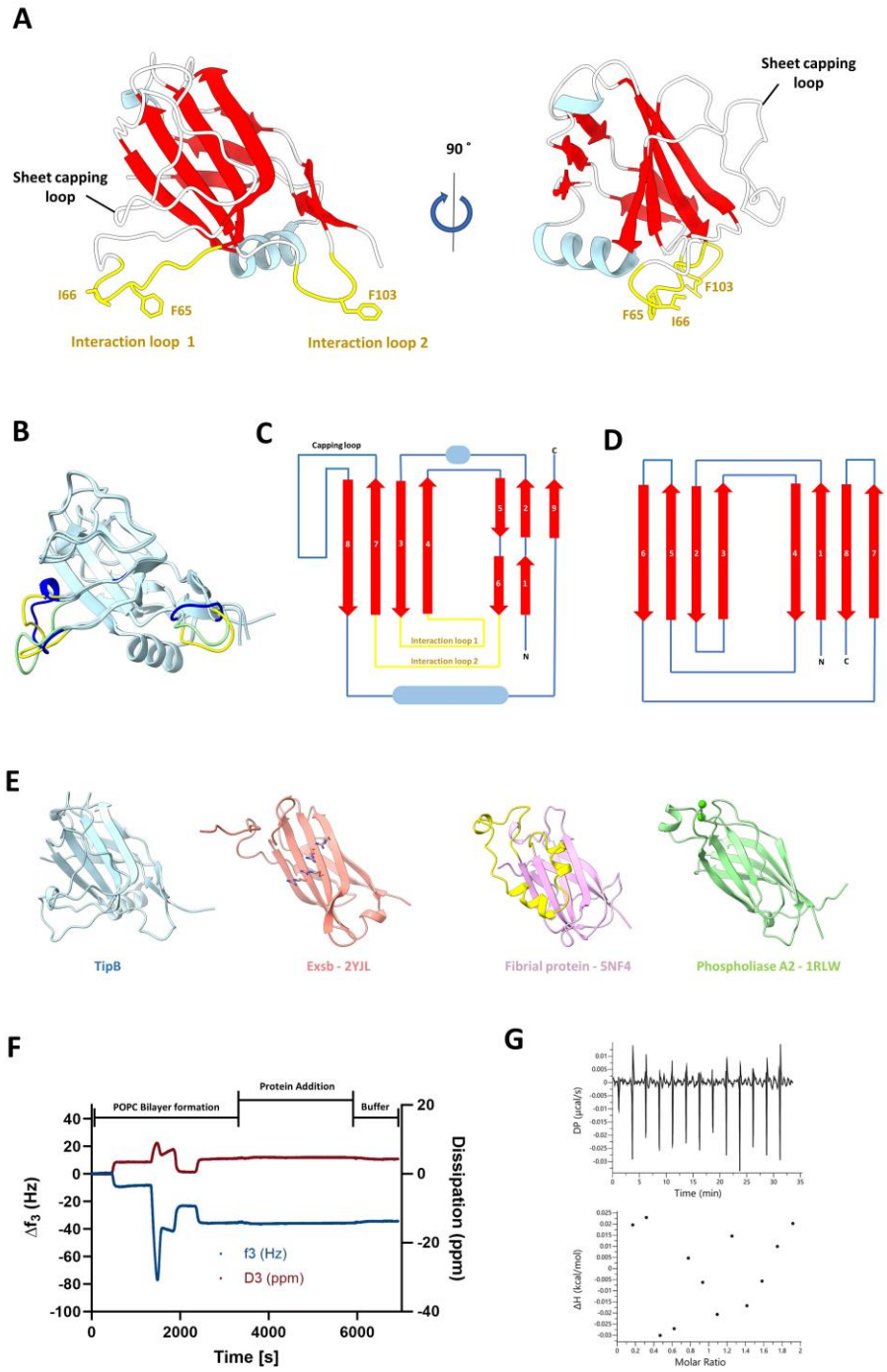

Figure 3. Crystal structure of the TipB adapter protein

(A) Crystal structure of TipB, coloured by secondary structure (beta – red, helix – light blue, coil – white) with the two specialised interaction loops coloured yellow. Key hydrophobic amino acids in the interaction loops are shown in stick form. **(B)** The three chains of TipB in the ASU are superposed to highlight flexibility in the interaction loops (shown blue, green and yellow for each chain). **(C)** The topology of TipB, with strands in red, helices as blue ovals and loops as blue lines. **(D)** The topology of type II C2 domains. **(E)** Crystal structures of proteins identified in structural homology searches with DALI [24], shown in same orientation as TipB (left, light blue). Arginines that form the basic face of the sheet in *Pseudomonas aeruginosa* ExsB [26] (coloured salmon) are shown in stick form; the sheet capping loop of *Porphyromonas gingivalis* [53] (coloured pink) is shown in yellow; and the two calcium ions of human phospholipase A2 [35] (coloured green) are shown as

spheres. **(F)** QCM-D trace showing f3 and d3 signals. Upon protein addition, no significant change in f3 or d3 is observed. **(G)** ITC thermogram of a titration of calcium chloride into TipB showing no binding.

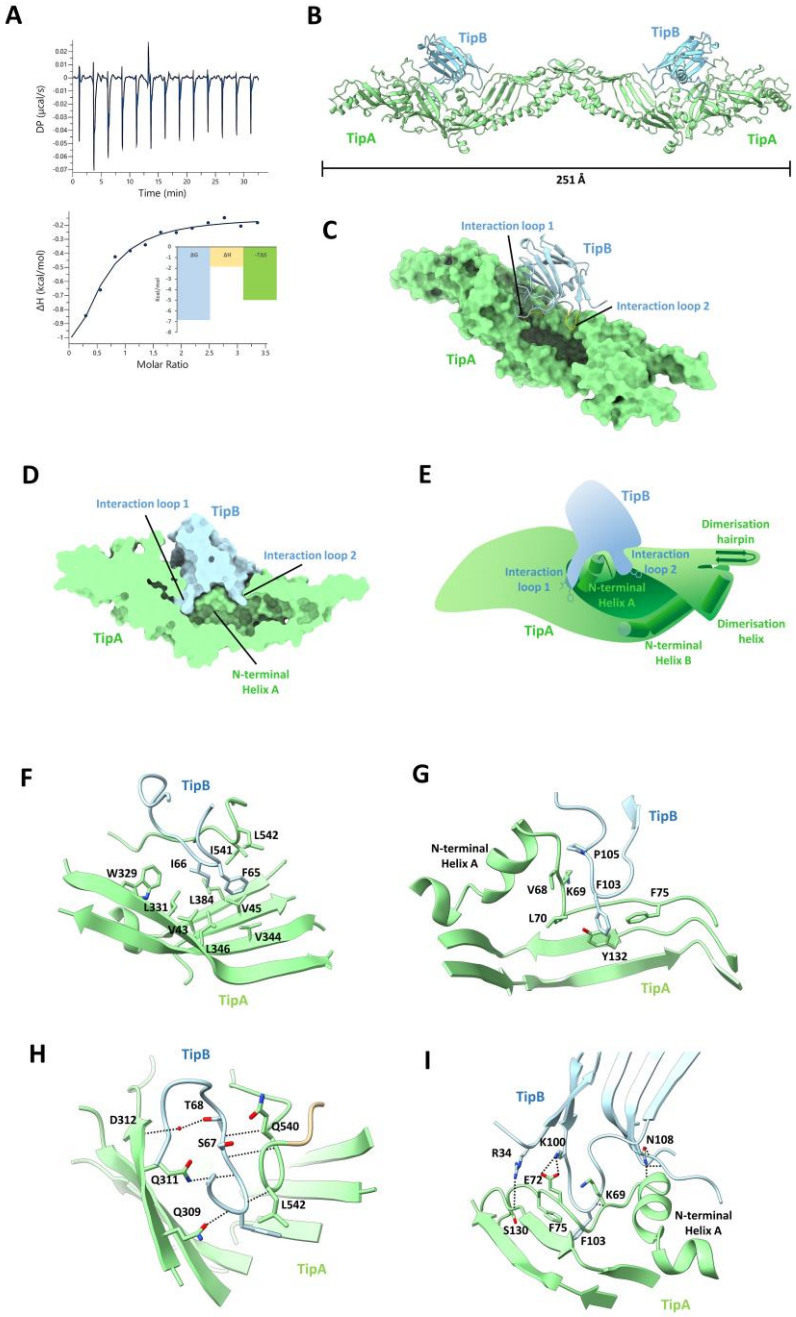

Figure 4. The interaction of the TipA and TipB TULIP:adapter pairing

(A) ITC thermogram of a titration of TipB into TipA, showing binding of the two proteins in solution. The reported energies for binding are shown as an embedded bar graph. **(B)** Crystal structure of the TipAB complex. Tip A is shown in green and forms the same 2-fold dimer as the isolated form through a crystallographic axis. TipB is shown in blue on top of TipA. **(C)** A surface view of TipA is shown, highlighting burial of the two interaction loops of TipB (coloured yellow). **(D)** A clipped surface view of the TipAB complex, showing TipA sat on the TipA N-terminal helix A. **(E)** A cartoon schematic of the interaction with parts of the TipA N-terminal TULIP domain secondary structure visible, and key hydrophobic residues of TipB shown as sticks. **(F)** Hydrophobic interactions of the TipB interaction loop 1. **(G)** Hydrophobic

interactions of the TipB interaction loop 2. **(H)** polar interactions of the TipB interaction loop 1. **(I)** Polar interactions of the TipB interaction loop 2.

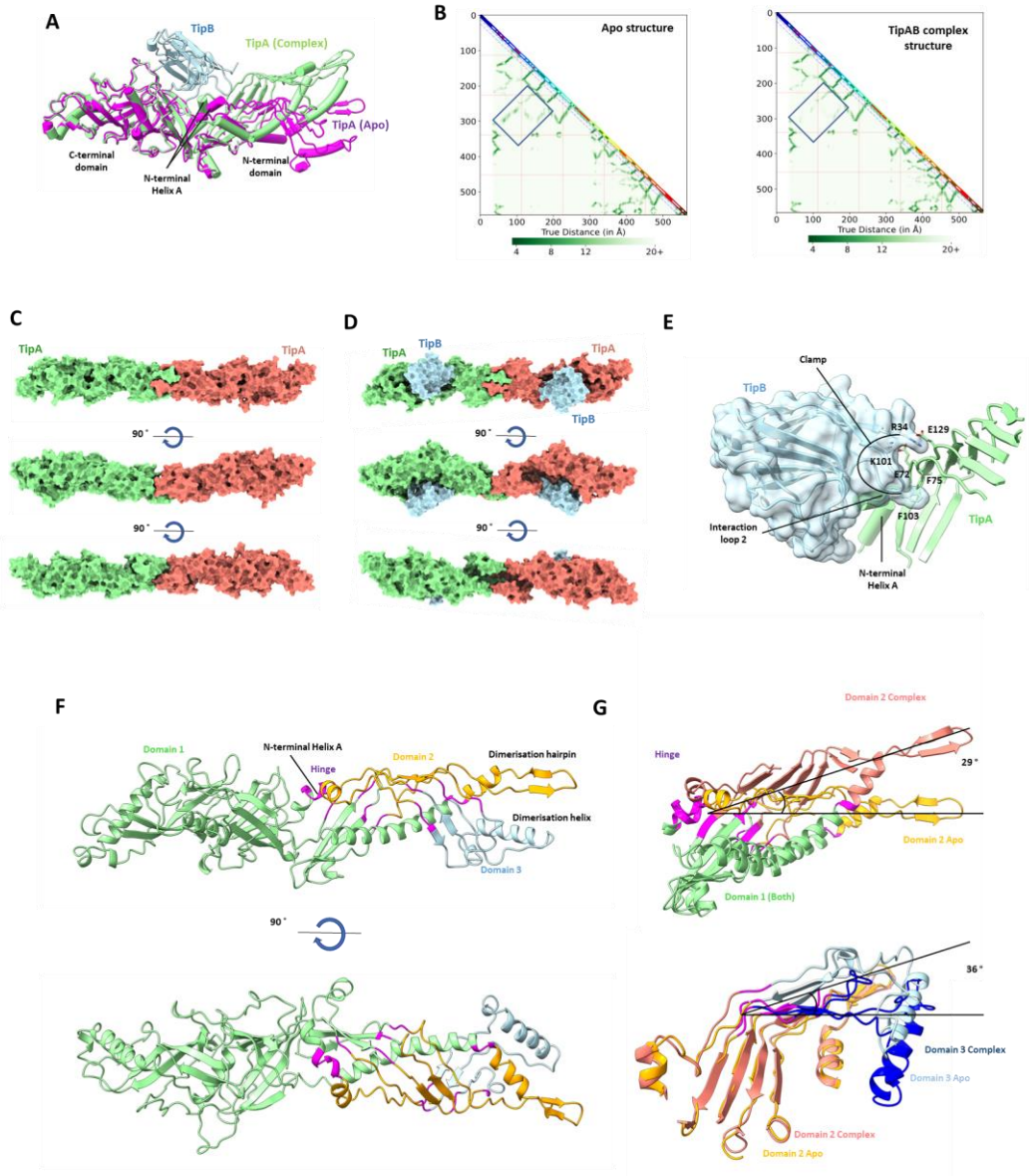

Figure 5. Conformational change of TipA when bound to the TipB adapter

(A) A superimposition of apo TipA (magenta) with the TipAB complex. Large motions in the N-terminal domain of TipA are visible. **(B)** contact plots of TipA for the apo TipA and TipAB structures, generated by DISTEVAL [54]. Both plots have a box surrounding residues that differ significantly between the two structures, which are only found in the N-terminal domain. **(C)** Three orientations of the apo TipA homodimer (one protomer green, one protomer red), showing a mostly-closed tube. **(D)** The same three orientations of the TipA homodimer as **(C)** for the TipAB complex. TipB is shown in blue, and the large opening of the TULIP homodimer stretching between the two TipB proteins is visible. **(E)** The clamp formed by interaction loop 2 and charged residues grasp the bottom and top of the TipA N-terminal beta sheet, respectively. **(F)** Analysis of the apo TipA and complexed TipA structure with DynDom to investigate the motions of the conformational change identifies three domains (coloured green, orange and blue), with motions in the hinge regions (magenta). **(G)** Upper; superpositions show the 29° rotation between Domain 1 and Domain 2 rotate by 29. Lower; superpositions show the 36° movement between domain 2 and domain 3.

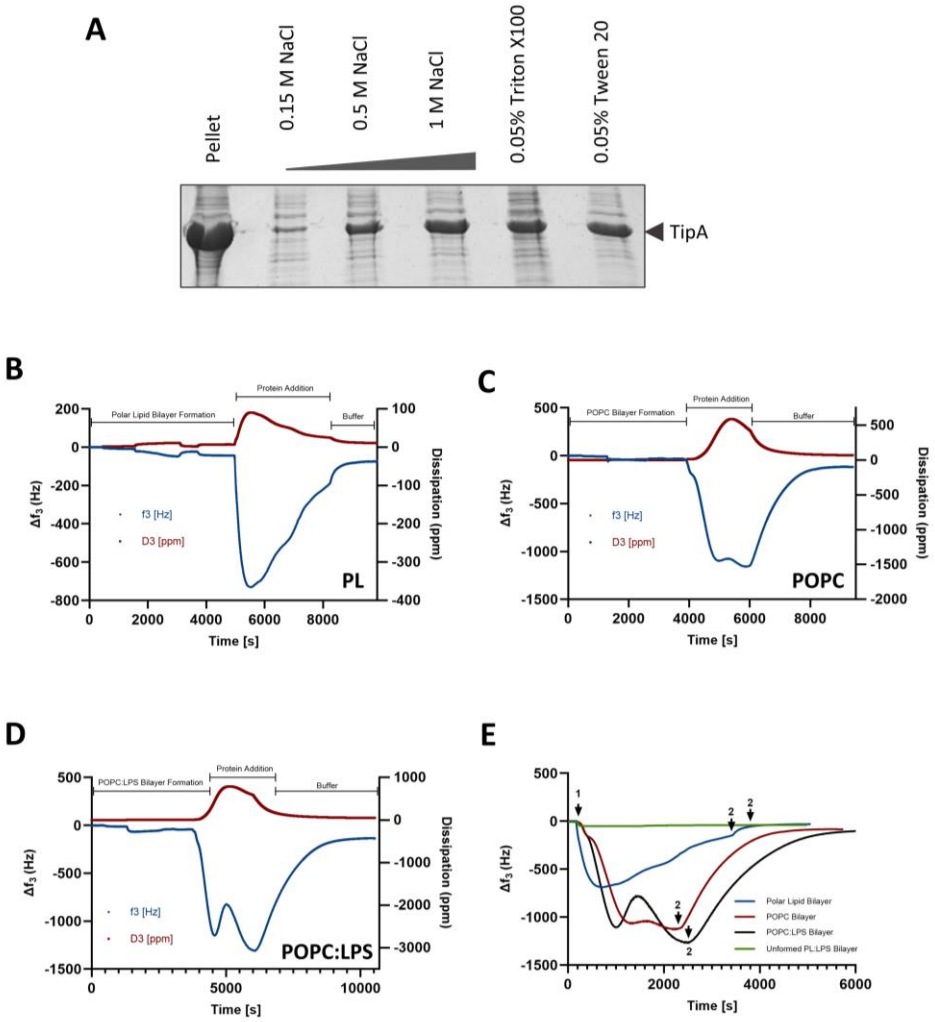

Figure 6. TipA can insert into a range of lipid bilayers

(A) Pellet-binding assays with TipA. SDS-PAGE of pellet and supernatants from various buffer washes. A prominent band for soluble TipA is observed in high salt concentrations or with the presence of detergents. **(B)** QCM-D measurements showing the changes in frequency (blue) and dissipation (red) in response to the mass deposition associated with *E. coli* polar lipid bilayer formation (polar lipid liposomes were deposited onto a silicon surface and ruptured through osmotic shock), followed by the addition of TipA, and subsequent bilayer washing with excess buffer. **(C)** QCM-D measurements as specified in **(A)** showing POPC bilayer formation, TipA addition, and buffer wash. **(D)** QCM-D measurements as specified in **(A)** indicating the formation of a stable POPC:LPS bilayer, TipA addition and subsequent buffer wash. **(E)** A comparison of the changes to frequency (indicative of mass changes), as measured through QCM-D, in response to the addition of TipA to various lipid bilayer compositions (1) and subsequent buffer wash (2). Note we were unable to successfully form a mixed polar lipid, LPS bilayer.

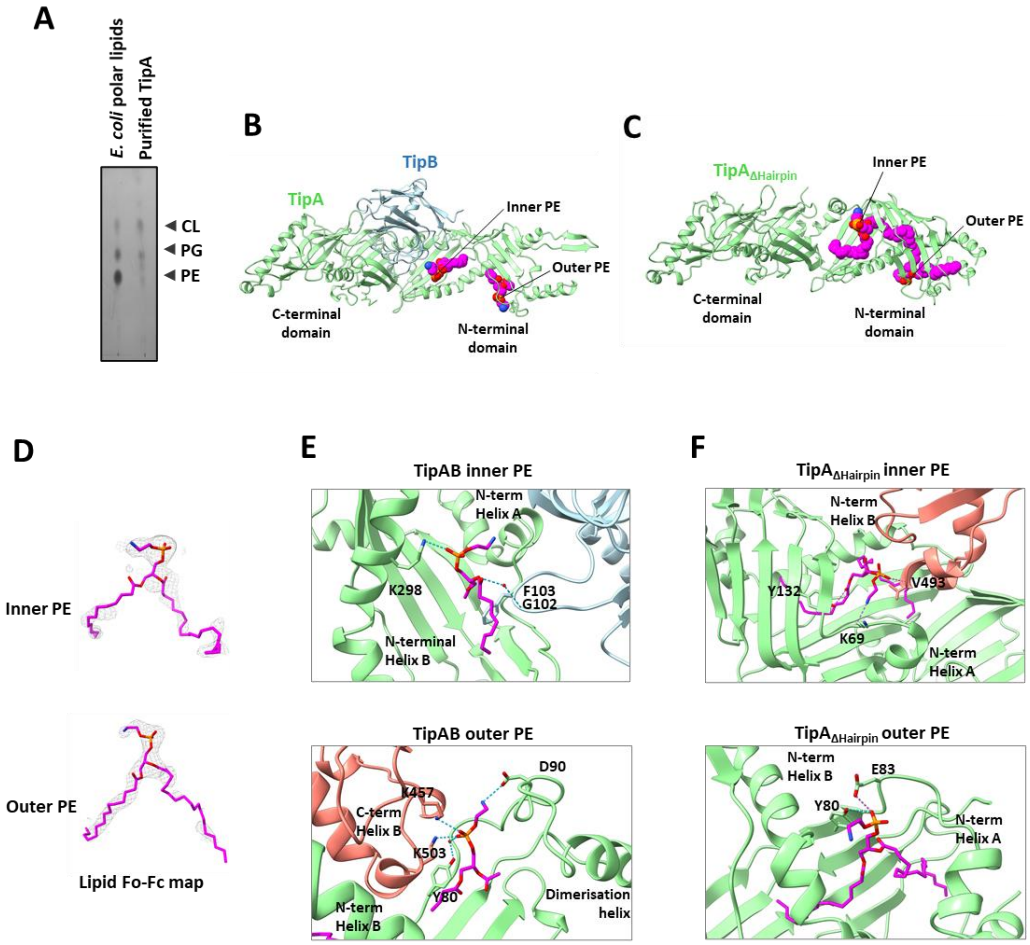

Figure 7. TipA sequesters lipids in the TULIP lumen

(A) TLC of lipids extracted from TipA. All three *E. coli* polar lipids are visible in the TipA lane (cardiolipin (CL), phosphatidylglycerol (PG), phosphatidylethanolamine (PE)), as are some additional species. **(B)** Crystal structure of the TipAB complex, with two lipid head groups shown as spheres (magenta carbons). **(C)** Crystal structure of TipA$_{\Delta Hairpin}$, with two modelled PE molecules shown as spheres (magenta carbons). **(D) 2**Fo-Fc electron density of the two lipids in the TipA$_{\Delta Hairpin}$ structure at 0.8 σ. **(E)** The molecular interactions of TipAB complex and the lipid head groups for the inner PE molecule (top) and outer PE molecule (bottom). TipA is coloured green, TipB is blue, with a symmetry TipA copy coloured salmon. Lipids are shown in stick form and coloured as heteroatoms (carbon – magenta, oxygen – red, nitrogen – blue, phosphorus – orange) **(F)** The molecular interactions of TipA$_{\Delta Hairpin}$ and the lipid head groups for the inner PE molecule (top) and outer PE molecule (bottom). TipA is coloured green with a symmetry TipA copy coloured salmon. Lipids are shown in stick form and coloured as heteroatoms (carbon – magenta, oxygen – red, nitrogen – blue, phosphorus – orange)

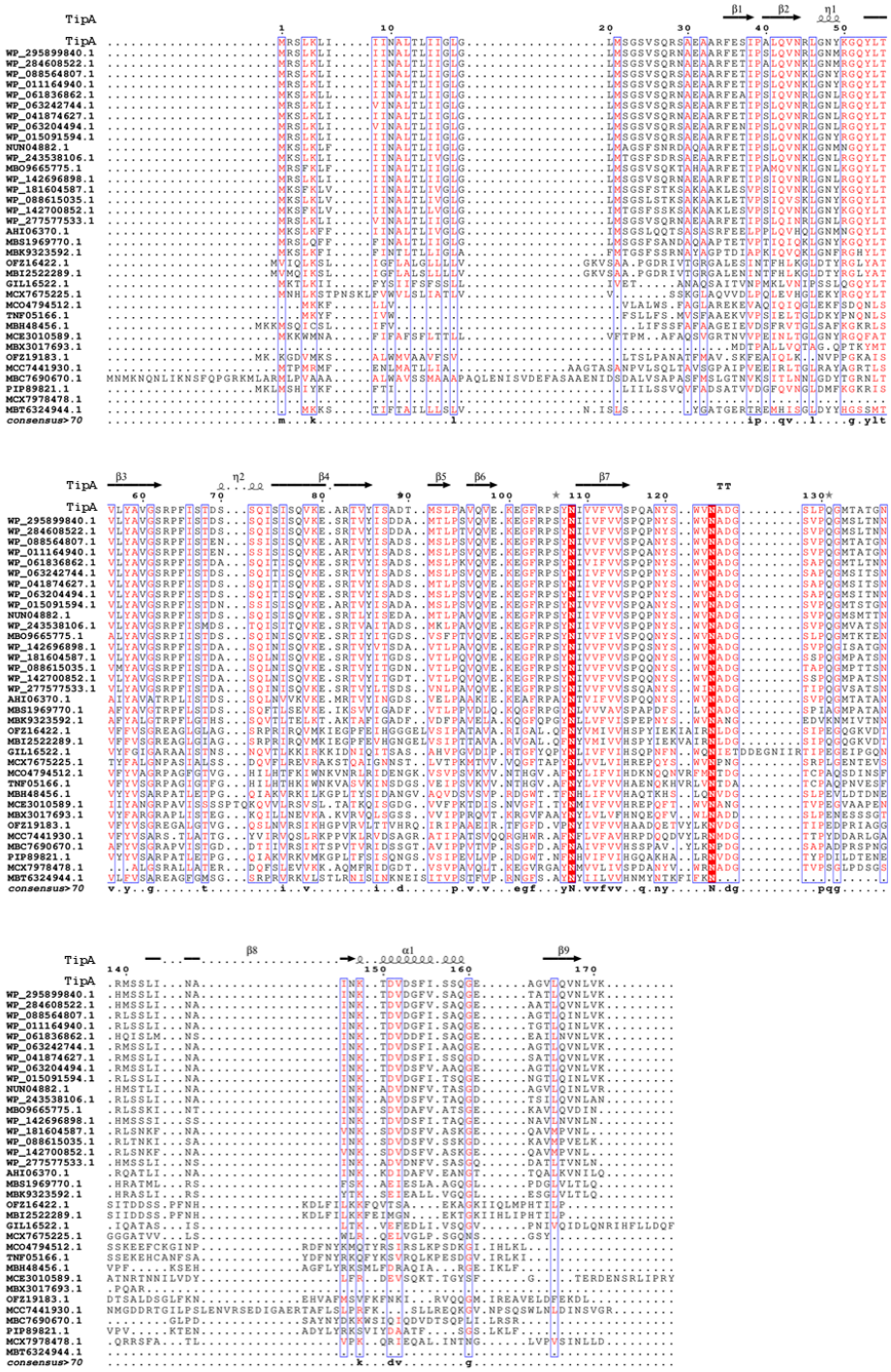

Figure EV1. Sequence alignments of TipA homologues

BlastP [55] was used to identify homologues to the *Bdellovibrio bacteriovorus* HD100 TipA protein. The only absolutely conserved residues are two Asn residiues. Alignments of the sequences obtained from blastp were made using Clustal Omega [56]. ESPRIPT [57] was used to visualise the alignement with secondary structure.

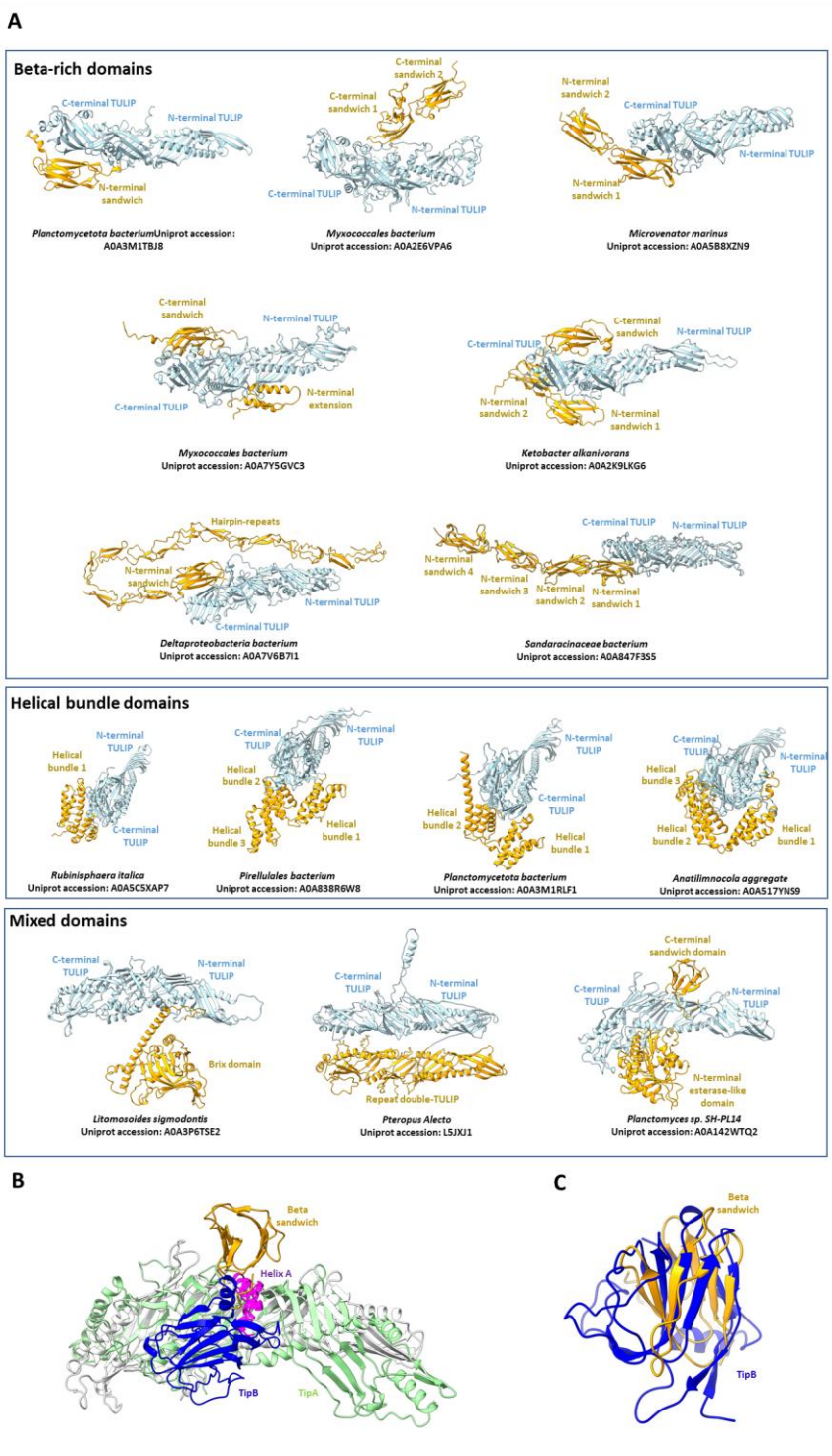

Figure EV2. Additional domains fused to TipA structural homologues

(A) Using Foldseek [38], structural TipA homologues were identified within the AlphaFold [58] AFDB50 database. A number of those homologues had additional domains to the double-TULIP. Representative examples of fusions are shown and comprise beta-rich domains (upper) helical domains (middle) and other domains including second double-TULIPs and enzymes (lower). The double-TULIP domains are coloured light blue, and the accessory domains are coloured orange. Of particular interest is the *Planctomyces sp*. SH-PL14 protein (bottom right) in which there is a similar beta-sandwich domain to TipB fused C-terminally to the TULIP **(B)** Superposition of the TipAB with *Planctomyces sp*. SH-PL14 (Uniprot accession: A0A142WTQ2). TipA is coloured green, TipB is blue, the TULIP domains of A0A142WTQ2 are white and the beta sandwich is orange. The enzymatic domain has been removed for clarity. The beta-sandwiches interact with the N-terminal Helix A in both structures and make interactions with the top of the N-terminal TULIP sheet. **(C)** Superposition of TipB (blue) with the beta sandwich of A0A142WTQ2 (orange), showing similar topology.

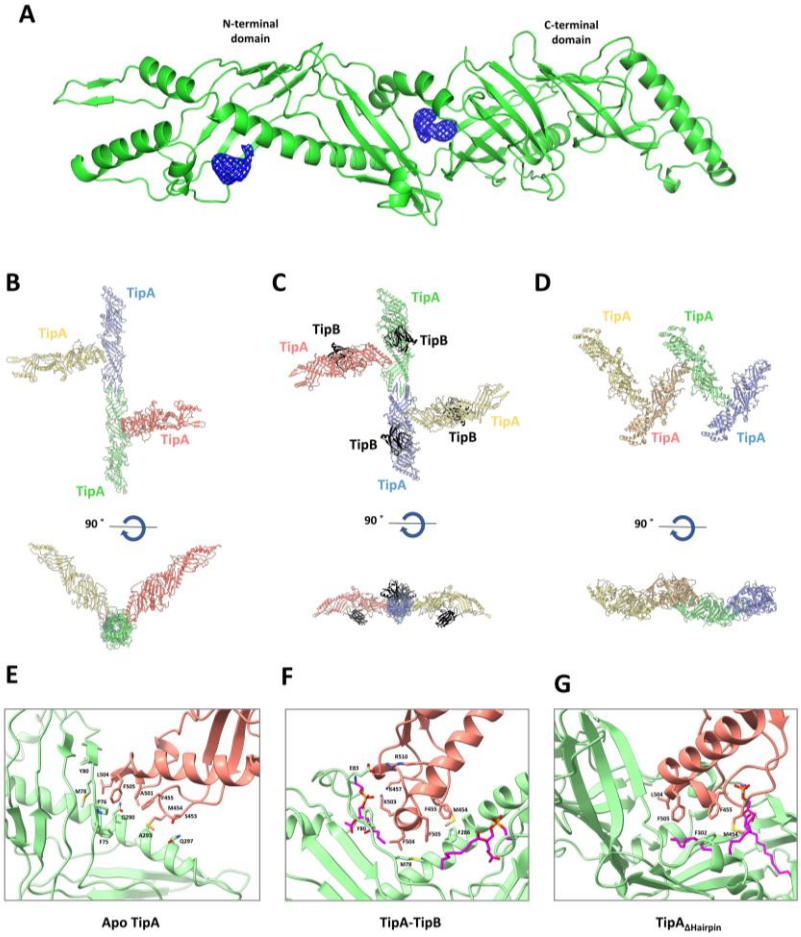

760 **Figure EV3. Lipid binding and higher order packing of TipA(A)** Fo-Fc electron density (blue mesh)
761 observed in the apo selenomethionine TipA structure. Large peaks are observed in similar regions to lipid density in the TipAB complex and
762 TipA$_{\Delta Hairpin}$. **(B)** Crystal packing in the apo selenomethionine structure. **(C)** Crystal packing in the TipAB complex structure. **(D)** Crystal
763 packing in the TipA$_{\Delta Hairpin}$ structure. In all structures shown **(B-D)** the C-terminal domain of TipA buries into the N-terminal domain of another
764 TipA protein. **(E)** Molecular interactions of the C-terminal domain and N-terminal of the apo selenomethionine TipA structure. **(F)** Molecular
765 interactions of the C-terminal domain and N-terminal of the TipAB structure. **(G)** Molecular interactions of the C-terminal domain and N-
766 terminal of the TipA$_{\Delta Hairpin}$ structure.

767
768
769

770 **Table EV1. Data collection and refinement statistics**

	Apo SeMet TipA	TipB	TipAB complex	TipA$_{\Delta Hairpin}$
Wavelength		0.979 Å	0.968 Å	0.968 Å
Resolution range	48.74 - 4.046 (4.191 - 4.046)	29.24 - 2.17 (2.23 - 2.17)	57.66 - 2.6 (2.693 - 2.6)	66.01 - 2.6 (2.72 - 2.6)
Space group	P 31 2 1	C 2 2 21	C 2 2 21	P 21 21 21
Unit cell	252.415 252.415 181.058 90 90 120	106.578 126.162 77.975 90 90 90	89.2741 230.652 131.606 90 90 90	57.9688 97.8339 132.021 90 90 90
Total reflections		376137	596458	307502
Unique reflections	45222 (538)	28055 (2231)	42141 (4178)	23555 (2618)
Multiplicity		13.4 (11.7)	14.1 (13.7)	13.1 (9.0)
Completeness (%)	82.85 (9.99)	99.30 (91.9)	98.36 (85.22)	98.8 (91.5)
Mean I/sigma(I)		16.8 (3.3)	11.6 (0.3)	18.6 (2.7)
Wilson B-factor	188.01	35.30	86.67	60.45
R-merge		0.102 (0.733)	0.117 (3.31)	0.083 (0.681)
R-meas		0.110 (0.798)	0.125 (3.55)	0.089 (0.770)
R-pim		0.041 (0.312)	0.034 (0.946)	0.033 (0.350)
CC1/2		0.999 (0.896)	0.999 (0.333)	0.999 (0.832)
Reflections used in refinement	45184 (538)	28025 (2640)	41504 (3563)	23500 (2098)
Reflections used for R-free	2364 (23)	1360 (115)	2105 (196)	1132 (117)
R-work	0.2766 (0.4538)	0.1774 (0.2220)	0.2463 (0.3946)	0.2283 (0.2910)
R-free	0.3200 (0.5542)	0.2160 (0.2798)	0.2874 (0.4209)	0.2526 (0.3627)
Number of non-hydrogen atoms	12575	3394	5382	4178
macromolecules	12575	3196	5267	3990
ligands	0	0	55	135
solvent	0	198	60	53
Protein residues	1600	415	674	507
RMS(bonds)	0.005	0.009	0.005	0.007
RMS(angles)	1.33	1.01	0.75	1.04
Ramachandran favored (%)	79.99	96.58	94.48	93.01
Ramachandran allowed (%)	18.51	2.93	5.07	6.39
Ramachandran outliers (%)	1.51	0.49	0.45	0.60
Rotamer outliers (%)	0.58	0.55	2.25	3.22
Clashscore	30.35	5.33	12.23	13.31
Average B-factor	239.19	45.22	110.85	83.37
macromolecules	239.19	45.05	111.03	83.25
ligands			115.13	96.48
solvent		47.96	91.11	59.35
Number of TLS groups	1	1	16	1

771 Statistics for the highest-resolution shell are shown in parentheses.

772

773

774

775

776

777

778

779

References

1. Negus, D., et al., *Predator Versus Pathogen: How Does Predatory Bdellovibrio bacteriovorus Interface with the Challenges of Killing Gram-Negative Pathogens in a Host Setting?* Annu Rev Microbiol, 2017. **71**: p. 441-457.
2. Bratanis, E., et al., *Biotechnological Potential of Bdellovibrio and Like Organisms and Their Secreted Enzymes.* Front Microbiol, 2020. **11**: p. 662.
3. Rendulic, S., et al., *A predator unmasked: life cycle of Bdellovibrio bacteriovorus from a genomic perspective.* Science, 2004. **303**(5658): p. 689-92.
4. Matin, A. and S.C. Rittenberg, *Kinetics of deoxyribonucleic acid destruction and synthesis during growth of Bdellovibrio bacteriovorus strain 109D on pseudomonas putida and escherichia coli.* J Bacteriol, 1972. **111**(3): p. 664-73.
5. Hespell, R.B., G.F. Miozzari, and S.C. Rittenberg, *Ribonucleic acid destruction and synthesis during intraperiplasmic growth of Bdellovibrio bacteriovorus.* J Bacteriol, 1975. **123**(2): p. 481-91.
6. Thomashow, M.F. and S.C. Rittenberg, *Intraperiplasmic growth of Bdellovibrio bacteriovorus 109J: solubilization of Escherichia coli peptidoglycan.* J Bacteriol, 1978. **135**(3): p. 998-1007.
7. Rosson, R.A. and S.C. Rittenberg, *Regulated breakdown of Escherichia coli deoxyribonucleic acid during intraperiplasmic growth of Bdellovibrio bacteriovorus 109J.* J Bacteriol, 1979. **140**(2): p. 620-33.
8. Nelson, D.R. and S.C. Rittenberg, *Incorporation of substrate cell lipid A components into the lipopolysaccharide of intraperiplasmically grown Bdellovibrio bacteriovorus.* J Bacteriol, 1981. **147**(3): p. 860-8.
9. Kuenen, J.G. and S.C. Rittenberg, *Incorporation of long-chain fatty acids of the substrate organism by Bdellovibrio bacteriovorus during intraperiplasmic growth.* J Bacteriol, 1975. **121**(3): p. 1145-57.
10. Abram, D., J. Castro e Melo, and D. Chou, *Penetration of Bdellovibrio bacteriovorus into host cells.* J Bacteriol, 1974. **118**(2): p. 663-80.
11. Banks, E.J., et al., *Asymmetric peptidoglycan editing generates cell curvature in Bdellovibrio predatory bacteria.* Nat Commun, 2022. **13**(1): p. 1509.
12. Kuru, E., et al., *Fluorescent D-amino-acids reveal bi-cellular cell wall modifications important for Bdellovibrio bacteriovorus predation.* Nat Microbiol, 2017. **2**(12): p. 1648-1657.
13. Giacometti, S.I., et al., *Lipid Transport Across Bacterial Membranes.* Annu Rev Cell Dev Biol, 2022. **38**: p. 125-153.
14. Reinisch, K.M. and P. De Camilli, *SMP-domain proteins at membrane contact sites: Structure and function.* Biochim Biophys Acta, 2016. **1861**(8 Pt B): p. 924-927.
15. Alva, V. and A.N. Lupas, *The TULIP superfamily of eukaryotic lipid-binding proteins as a mediator of lipid sensing and transport.* Biochim Biophys Acta, 2016. **1861**(8 Pt B): p. 913-923.
16. Wong, L.H. and T.P. Levine, *Tubular lipid binding proteins (TULIPs) growing everywhere.* Biochim Biophys Acta Mol Cell Res, 2017. **1864**(9): p. 1439-1449.
17. Levine, T.P., *Remote homology searches identify bacterial homologues of eukaryotic lipid transfer proteins, including Chorein-N domains in TamB and AsmA and Mdm31p.* BMC Mol Cell Biol, 2019. **20**(1): p. 43.
18. Barrio-Hernandez, I., et al., *Clustering predicted structures at the scale of the known protein universe.* Nature, 2023. **622**(7983): p. 637-645.

19. Gustafsson, R., et al., *Crystal structures of OrfX2 and P47 from a Botulinum neurotoxin OrfX-type gene cluster.* FEBS Lett, 2017. **591**(22): p. 3781-3792.
20. Gao, L., et al., *Crystal structures of OrfX1, OrfX2 and the OrfX1-OrfX3 complex from the orfX gene cluster of botulinum neurotoxin E1.* FEBS Lett, 2023. **597**(4): p. 524-537.
21. Lambert, C., et al., *The first bite--profiling the predatosome in the bacterial pathogen Bdellovibrio.* PLoS One, 2010. **5**(1): p. e8599.
22. Tyson, J., et al., *Prey killing without invasion by Bdellovibrio bacteriovorus defective for a MIDAS-family adhesin.* Nat Commun, 2024. **15**(1): p. 3078.
23. Paysan-Lafosse, T., et al., *InterPro in 2022.* Nucleic Acids Res, 2023. **51**(D1): p. D418-D427.
24. Holm, L., *Dali server: structural unification of protein families.* Nucleic Acids Res, 2022. **50**(W1): p. W210-W215.
25. Voss, N.R. and M. Gerstein, *3V: cavity, channel and cleft volume calculator and extractor.* Nucleic Acids Res, 2010. **38**(Web Server issue): p. W555-62.
26. Izore, T., et al., *Structural characterization and membrane localization of ExsB from the type III secretion system (T3SS) of Pseudomonas aeruginosa.* J Mol Biol, 2011. **413**(1): p. 236-46.
27. Nalefski, E.A. and J.J. Falke, *The C2 domain calcium-binding motif: structural and functional diversity.* Protein Sci, 1996. **5**(12): p. 2375-90.
28. Kohout, S.C., et al., *C2 domains of protein kinase C isoforms alpha, beta, and gamma: activation parameters and calcium stoichiometries of the membrane-bound state.* Biochemistry, 2002. **41**(38): p. 11411-24.
29. Nalefski, E.A., et al., *Delineation of two functionally distinct domains of cytosolic phospholipase A2, a regulatory Ca(2+)-dependent lipid-binding domain and a Ca(2+)-independent catalytic domain.* J Biol Chem, 1994. **269**(27): p. 18239-49.
30. Saheki, Y. and P. De Camilli, *The Extended-Synaptotagmins.* Biochim Biophys Acta Mol Cell Res, 2017. **1864**(9): p. 1490-1493.
31. Dixon, M.C., *Quartz crystal microbalance with dissipation monitoring: enabling real-time characterization of biological materials and their interactions.* J Biomol Tech, 2008. **19**(3): p. 151-8.
32. Hughes, G.W., et al., *Evidence for phospholipid export from the bacterial inner membrane by the Mla ABC transport system.* Nat Microbiol, 2019. **4**(10): p. 1692-1705.
33. Richter, R., A. Mukhopadhyay, and A. Brisson, *Pathways of lipid vesicle deposition on solid surfaces: a combined QCM-D and AFM study.* Biophys J, 2003. **85**(5): p. 3035-47.
34. Shen, H.H., et al., *Reconstitution of a nanomachine driving the assembly of proteins into bacterial outer membranes.* Nat Commun, 2014. **5**: p. 5078.
35. Perisic, O., et al., *Crystal structure of a calcium-phospholipid binding domain from cytosolic phospholipase A2.* J Biol Chem, 1998. **273**(3): p. 1596-604.
36. Krissinel, E. and K. Henrick, *Inference of macromolecular assemblies from crystalline state.* J Mol Biol, 2007. **372**(3): p. 774-97.
37. Lee, R.A., M. Razaz, and S. Hayward, *The DynDom database of protein domain motions.* Bioinformatics, 2003. **19**(10): p. 1290-1.
38. van Kempen, M., et al., *Fast and accurate protein structure search with Foldseek.* Nat Biotechnol, 2024. **42**(2): p. 243-246.
39. Schauder, C.M., et al., *Structure of a lipid-bound extended synaptotagmin indicates a role in lipid transfer.* Nature, 2014. **510**(7506): p. 552-5.
40. AhYoung, A.P., et al., *Conserved SMP domains of the ERMES complex bind phospholipids and mediate tether assembly.* Proc Natl Acad Sci U S A, 2015. **112**(25): p. E3179-88.

41. Ekiert, D.C., et al., *Architectures of Lipid Transport Systems for the Bacterial Outer Membrane.* Cell, 2017. **169**(2): p. 273-285 e17.
42. Kumar, S. and N. Ruiz, *Bacterial AsmA-Like Proteins: Bridging the Gap in Intermembrane Phospholipid Transport.* Contact (Thousand Oaks), 2023. **6**: p. 25152564231185931.
43. Yu, H., et al., *Extended synaptotagmins are Ca2+-dependent lipid transfer proteins at membrane contact sites.* Proc Natl Acad Sci U S A, 2016. **113**(16): p. 4362-7.
44. Jeong, H., J. Park, and C. Lee, *Crystal structure of Mdm12 reveals the architecture and dynamic organization of the ERMES complex.* EMBO Rep, 2016. **17**(12): p. 1857-1871.
45. Suzuki, R., et al., *Structural mechanism of JH delivery in hemolymph by JHBP of silkworm, Bombyx mori.* Sci Rep, 2011. **1**: p. 133.
46. Weiss, J., et al., *Purification and characterization of a potent bactericidal and membrane active protein from the granules of human polymorphonuclear leukocytes.* J Biol Chem, 1978. **253**(8): p. 2664-72.
47. Toulmay, A. and W.A. Prinz, *A conserved membrane-binding domain targets proteins to organelle contact sites.* J Cell Sci, 2012. **125**(Pt 1): p. 49-58.
48. Mirdita, M., et al., *ColabFold: making protein folding accessible to all.* Nat Methods, 2022. **19**(6): p. 679-682.
49. McCoy, A.J., *Solving structures of protein complexes by molecular replacement with Phaser.* Acta Crystallogr D Biol Crystallogr, 2007. **63**(Pt 1): p. 32-41.
50. Emsley, P. and K. Cowtan, *Coot: model-building tools for molecular graphics.* Acta Crystallogr D Biol Crystallogr, 2004. **60**(Pt 12 Pt 1): p. 2126-32.
51. Afonine, P.V., et al., *Towards automated crystallographic structure refinement with phenix.refine.* Acta Crystallogr D Biol Crystallogr, 2012. **68**(Pt 4): p. 352-67.
52. Sehnal, D., et al., *MOLE 2.0: advanced approach for analysis of biomacromolecular channels.* J Cheminform, 2013. **5**(1): p. 39.
53. Hall, M., et al., *Structural and functional characterization of shaft, anchor, and tip proteins of the Mfa1 fimbria from the periodontal pathogen Porphyromonas gingivalis.* Sci Rep, 2018. **8**(1): p. 1793.
54. Adhikari, B., et al., *DISTEVAL: a web server for evaluating predicted protein distances.* BMC Bioinformatics, 2021. **22**(1): p. 8.
55. Altschul, S.F., et al., *Basic local alignment search tool.* J Mol Biol, 1990. **215**(3): p. 403-10.
56. Sievers, F. and D.G. Higgins, *Clustal Omega for making accurate alignments of many protein sequences.* Protein Sci, 2018. **27**(1): p. 135-145.
57. Robert, X. and P. Gouet, *Deciphering key features in protein structures with the new ENDscript server.* Nucleic Acids Res, 2014. **42**(Web Server issue): p. W320-4.
58. Jumper, J., et al., *Highly accurate protein structure prediction with AlphaFold.* Nature, 2021. **596**(7873): p. 583-589.

Acknowledgements

ALL, SGC, and ITC were funded by the Wellcome Trust Investigator Award in Science (209437/Z/17/Z); AL and SGC acknowledge additional funding from a BBSRC award (BB/X006298/1). GH and TJK were funded by BBSRC award BB/S017283/1, and HJ by BBSRC studentship BB/T00746X/1. We are grateful to Paul Radford and Liz Sockett for attempts to monitor functional role and localization in vivo. We thank Diamond Light Source for beamtime and for facility support during data collection.